Secretion of VGF relies on the interplay between LRRK2 and post-Golgi v-SNAREs

Francesca Filippini, Sébastien Nola, Ahmed Zahraoui, Kevin Roger, Mansoore Esmaili, Ji Sun, José Wojnacki, Anaïs Vlieghe, Philippe Bun, Stéphanie Blanchon, et al.

Cell Reports

Article

Secretion of VGF relies on the interplay between LRRK2 and post-Golgi v-SNAREs

Graphical abstract

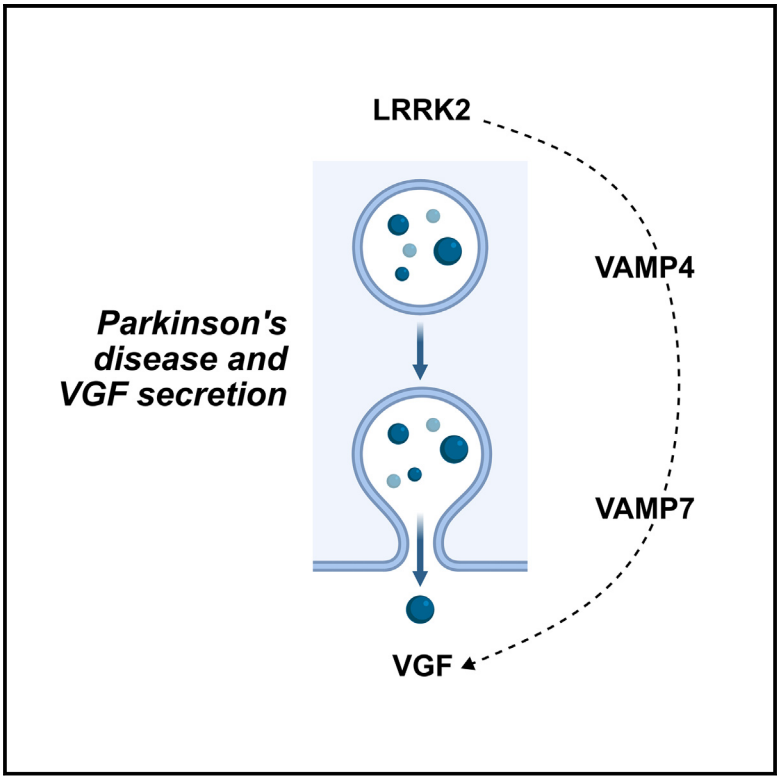

Authors

Francesca Filippini, Sébastien Nola, Ahmed Zahraoui, ..., Marie-Christine Chartier-Harlin, Chiara Guerrera, Thierry Galli

Correspondence

thierry.galli@inserm.fr

In brief

Filippini et al. report the direct interaction of leucine-rich repeat kinase 2 (LRRK2) with the endosomal vesicular SNAREs VAMP4 and VAMP7. LRRK2, VAMP4, and VAMP7 regulate the secretion of the Parkinson's disease biomarker VGF. They provide evidence for the role of LRRK2 in regulating unconventional secretion in the disease.

Highlights

- LRRK2 interacts with the endosomal v-SNAREs VAMP4 and VAMP7
- VAMP4 and VAMP7 mediate the secretion of the Parkinson's disease biomarker VGF
- LRRK2 regulates the accumulation vs. secretion of VGF

Filippini et al., 2023, Cell Reports *42*, 112221
March 28, 2023
https://doi.org/10.1016/j.celrep.2023.112221

CellPress

Cell Reports

CellPress
OPEN ACCESS

Article

Secretion of VGF relies on the interplay between LRRK2 and post-Golgi v-SNAREs

Francesca Filippini,[1,8,10] Sébastien Nola,[1,10] Ahmed Zahraoui,[1] Kevin Roger,[2] Mansoore Esmaili,[3] Ji Sun,[3] José Wojnacki,[1,9] Anaïs Vlieghe,[1] Philippe Bun,[4] Stéphanie Blanchon,[5] Jean-Christophe Rain,[5] Jean-Marc Taymans,[6] Marie-Christine Chartier-Harlin,[6] Chiara Guerrera,[2] and Thierry Galli[1,7,11,*]

[1]Université Paris Cité, Institute of Psychiatry and Neuroscience of Paris, INSERM U1266, Membrane Traffic in Healthy & Diseased Brain, 75014 Paris, France
[2]Université Paris Cité, Proteomics Platform Necker, Structure Fédérative de Recherche Necker, INSERM US24/CNRS UMS3633, 75015 Paris, France
[3]Department of Structural Biology, St. Jude Children's Research Hospital, Memphis, TN 38105, USA
[4]Université Paris Cité, Institute of Psychiatry and Neuroscience of Paris (IPNP), INSERM U1266, NeurImag Imaging Facility, 75014 Paris, France
[5]Hybrigenics Services, 91000 Évry-Courcouronnes, France
[6]Université de Lille, INSERM, CHU Lille, UMR-S1172, LilNCog – Lille Neuroscience & Cognition, Lille, France
[7]GHU Paris Psychiatrie & Neurosciences, Paris, France
[8]Present address: Department of Cell Biology, Yale University School of Medicine, New Haven, CT 06510, USA
[9]Present address: Centre for Genomic Regulation, The Barcelona Institute of Science and Technology, 08003 Barcelona, Spain
[10]These authors contributed equally
[11]Lead contact
*Correspondence: thierry.galli@inserm.fr
https://doi.org/10.1016/j.celrep.2023.112221

SUMMARY

The neuropeptide VGF was recently proposed as a neurodegeneration biomarker. The Parkinson's disease-related protein leucine-rich repeat kinase 2 (LRRK2) regulates endolysosomal dynamics, a process that involves SNARE-mediated membrane fusion and could regulate secretion. Here we investigate potential biochemical and functional links between LRRK2 and v-SNAREs. We find that LRRK2 directly interacts with the v-SNAREs VAMP4 and VAMP7. Secretomics reveals VGF secretory defects in VAMP4 and VAMP7 knockout (KO) neuronal cells. In contrast, VAMP2 KO "regulated secretion-null" and ATG5 KO "autophagy-null" cells release more VGF. VGF is partially associated with extracellular vesicles and LAMP1+ endolysosomes. LRRK2 expression increases VGF perinuclear localization and impairs its secretion. Retention using selective hooks (RUSH) assays show that a pool of VGF traffics through VAMP4+ and VAMP7+ compartments, and LRRK2 expression delays its transport to the cell periphery. Overexpression of LRRK2 or VAMP7-longin domain impairs VGF peripheral localization in primary cultured neurons. Altogether, our results suggest that LRRK2 might regulate VGF secretion via interaction with VAMP4 and VAMP7.

INTRODUCTION

Parkinson's disease (PD) involves the progressive loss of dopaminergic neurons in the substantia nigra pars compacta, resulting in a loss of dopamine in basal ganglia with consequent motor and non-motor impairments. Genetic studies have revealed more than 20 genes or loci linked to familial forms of Parkinson's disease, and recent meta-analyses of genome-wide association studies have shown at least 90 independent risk-associated variants for PD,[1] carried by 10% of PD patients. The *PARK8* locus was first identified as a PD-linked locus in a family with autosomal-dominant PD[2] with incomplete penetrance and sequencing of the locus identified that mutations in the leucine-rich repeat kinase 2 (*LRRK2*) gene are responsible for *PARK8*-related PD.[3,4] *LRRK2* encodes for a large multidomain protein with a central enzymatic core composed of both a kinase and a GTPase domain,[5] in which are located the most common LRRK2-PD-related mutations. How those mutations are related to PD is still unclear, but several studies have reported impaired activity of both kinase and GTPase domain as hallmark of PD pathogenic phenotypes and mechanisms.[6] LRRK2 has been shown to regulate intracellular membrane trafficking, playing a role in autophagy-lysosomal pathway and modulating retrograde as well as anterograde post-Golgi transport.[7,8] Moreover, LRRK2 is associated with various intracellular membranes by interacting with lipids[9] and phosphorylating several Rab proteins involved in post-Golgi vesicular traffic.[10,11] LRRK2 belongs to the ROCO superfamily of proteins, which also includes LRRK1. These two proteins have a conserved enzymatic core and share a similar overall dimeric structure,[12] displaying interactomes that partially overlap.[13] We and others have previously described LRRK1 as a binding partner of VAMP7,[14,15] a post-Golgi

v-SNARE that mediates the fusion of vesicles derived from the Golgi apparatus (GA)[16,17] and late endosomal CD63+ compartments[18] with the plasma membrane, particularly in neurite growth.[19,20] CD63 is a marker of secretory endolysosomes and amphisomes.[21] Interestingly, our group has recently used mass spectrometry (MS) proteomics and secretomics to uncover that VAMP7 is required for the release of endoplasmic reticulum (ER)-phagy proteins such as RTN3 and autophagy proteins p62 and LC3-II in extracellular vesicles (EVs).[22] LRRK2 can be found in the Golgi-associated retrograde protein (GARP) complex together with VAMP4.[23] VAMP4 was found as a potential risk factor of PD in association with LRRK2.[24] VAMP4 is involved in retrograde transport from early endosomes to the GA,[25,26] and secretion[27,28] particularly of vesicles involved in neurite growth, in a process also involving VAMP7.[19,27,29,30]

The search for PD biomarkers has recently converged on the secreted peptide VGF/secretogranin (SG) VII, which was found to be associated with the disease in cerebrospinal fluid (CSF), blood, and urine.[31–33] This raises the hypothesis that secretory defects, not limited to dopamine release, might contribute to the disease.

In this study, we took advantage of our recent findings on the v-SNARE-dependent trafficking and secretory pathway to investigate whether LRRK2 interacts with VAMP7 and other v-SNAREs and if this interplay could alter the endolysosomal system. We found that LRRK2 interacted directly with the post-Golgi VAMP4 and VAMP7 as shown by co-immunoprecipitation and pull-down experiments. Proteomics of the secretome of PC12 cells knocked out for VAMP4 and VAMP7 identified that VGF was impaired in both knockout (KO) cell lines. These VGF secretion defects were confirmed by immunoblot on extracellular vesicle fractions. We went on to characterize the trafficking of VGF, particularly the role of LRRK2 expression, by using the retention using selective hooks (RUSH) assay, which makes it possible to synchronize and follow the transport of the cargo from the ER to the plasma membrane or extracellular space.[34] In non-neuronal cells, expression of LRRK2 resulted in impaired secretion of VGF and its accumulation in the perinuclear area, a phenotype that we also found in neurons. Altogether, these data support the hypothesis that the secretion of VGF, particularly its pro-peptide, is a LRRK2-dependent mechanism, regulated via its interaction with VAMP4 and VAMP7.

RESULTS

LRRK2 interacts with post-Golgi v-SNAREs

First, we investigated the potential interactions between LRRK2 and v-SNAREs. Here we took advantage of our collection of GFP-tagged v-SNAREs that includes presynaptic and early endosomal VAMP2 and VAMP3, TGN and endosomal VAMP4, late endosomal VAMP7, late endosomal and lysosomal VAMP8, and ER-Golgi-related YKT6 and Sec22b. Of note, VAMP3 and VAMP8 are not expressed in neurons according to the Protein Atlas (https://www.proteinatlas.org). We performed co-immunoprecipitation experiments using HEK293T cells co-transfected with mCherry-LRRK2 wild-type (WT) and our repertoire of GFP-tagged v-SNAREs (Figures 1A and 1B). We found that LRRK2 was strongly co-immunoprecipitated with a subset of post-Golgi v-SNAREs (i.e., VAMP4, VAMP7, and VAMP8) when normalizing the bound LRRK2 to the precipitated corresponding VAMP. Weak interactions were detected with VAMP2 and VAMP3 and no significant interactions with Sec22b and YKT6. Therefore, the observed efficiency of interaction was as follows: VAMP4> VAMP7> VAMP8> VAMP2=-VAMP3>> YKT6=Sec22b=GFP.

We then asked if this hierarchy of interaction was maintained in the case of PD-related LRRK2 mutants G2019S and R1441C. We used the same experimental procedure of co-immunoprecipitation from cell lysates of co-transfected HEK293T cells, expressing this time either mCherry-LRRK2-G2019S or mCherry-LRRK2-R1441C and GFP-tagged v-SNAREs. VAMP4 and VAMP7 were the strongest LRRK2 interactors, whereas residual interactions were detected with VAMP2 and undetectable with YKT6 (Figures 1C–1F). Interestingly, we found the most efficient LRRK2/VAMP4 association with the R1441C mutant when we compared WT and mutants in the same experiment (Figures 1G and 1H). Therefore, LRRK2/VAMP4 appeared as the most significant LRRK2/v-SNARE interaction, and it was particularly enhanced by the R1441C mutation in the ROC GTPase domain.

We then tested if the interaction between LRRK2 and VAMP4/7 was direct. To this end, we used GST pull-down experiments with GST-VAMP4, GST-VAMP7, and GST-Snapin as positive control, as previous studies have identified a direct LRRK2/Snapin interaction.[35] Assays were carried out with the same LRRK2 protein as used for cryoelectron microscopy (cryo-EM) experiments, which made it possible to resolve its structure.[36] We found that GST-Snapin, GST-VAMP4, and GST-VAMP7 were able to pull down LRRK2, while there was a residual binding to control GST (Figures 1I and 1J). Interestingly, VAMP7 was less efficient than VAMP4, similar to previous findings using co-immunoprecipitation.

We then searched for domains in LRRK2 that would interact with VAMP4 and VAMP7. To this end, we constructed a random cDNA library of 44,500 human LRRK2 fragments in a yeast two hybrid (Y2H) expression vector. As Snapin was previously shown to interact with LRRK2 in Y2H assay,[35] we screened our LRRK2 fragments library with Snapin as bait (Figures S1A and S1B). This yielded several fragments, the intersection of which suggested a region from 1,773 to 1,857 residues as the interaction domain (ID). ID sequence corresponds to a region located within the COR domain of LRRK2 (Figures S1C and 2D). Surprisingly, when used as bait in a screen, VAMP4 or VAMP7 did not interact with the fragments from the LRRK2 library, nor with ID in a 1-by-1 Y2H assay (Figure S1E). Altogether, we conclude that VAMP4 and VAMP7 directly interact with LRRK2 in a domain that differs from the linear domain of interaction of Snapin and likely corresponds to a tertiary structure.

In GST pull-down assays on overexpressing HEK293T cells lysates, we observed that interaction of VAMP4 with LRRK2 was not altered by addition of Snapin (Figure S1F). Furthermore, using sequential co-immunoprecipitations first by pulling down GFP-Snapin then LRRK2, we were able to demonstrate that LRRK2, Snapin, and VAMP4 could be found together in the same poorly abundant protein complex (Figure S1G). These data suggest that LRRK2/VAMP4 and LRRK2/Snapin interactions are likely not mutually exclusive.

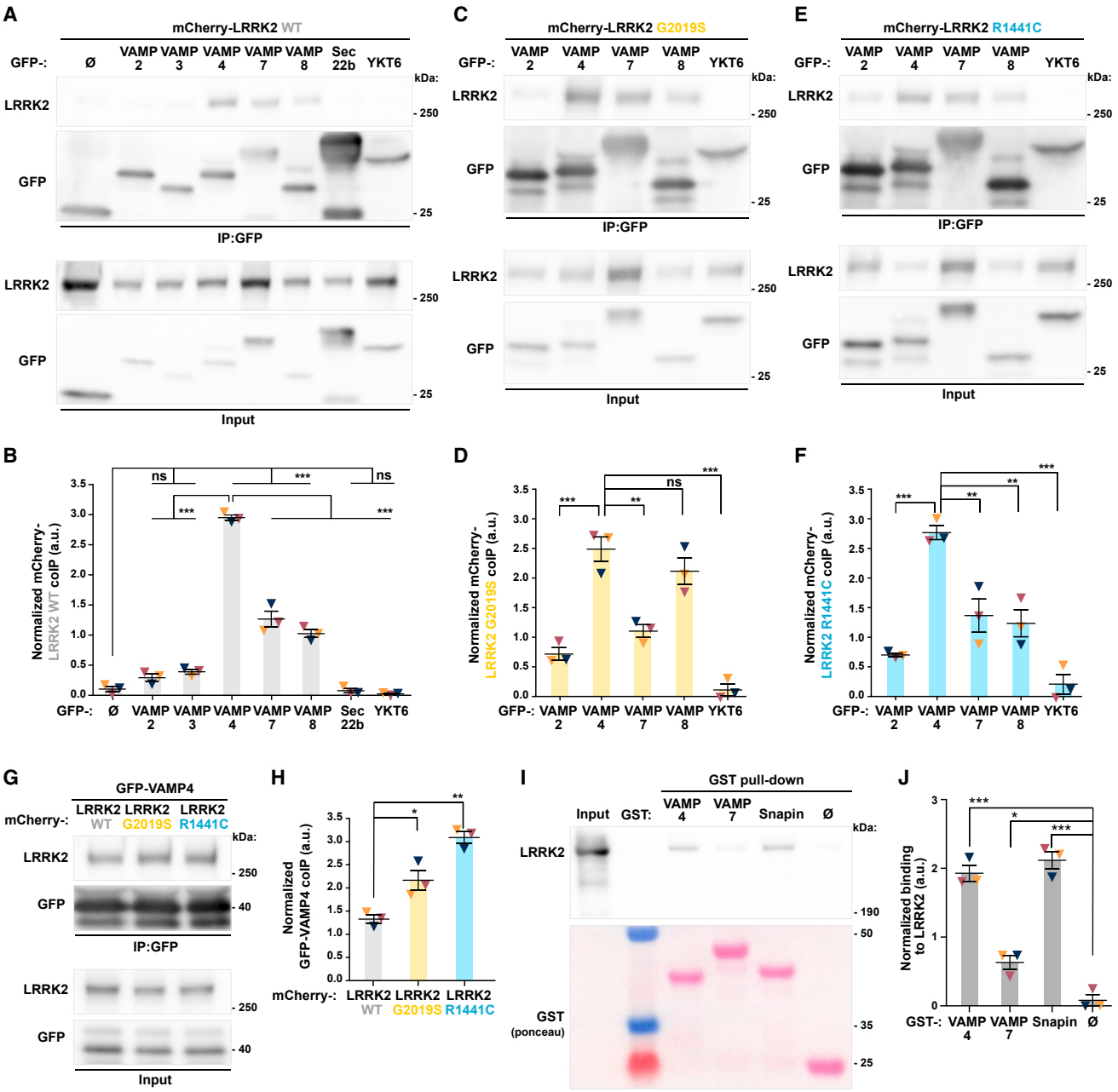

Figure 1. LRRK2 interacts with VAMP4, VAMP7, and VAMP8

(A, C, E, and G) HEK293T cells were co-transfected with mCherry-tagged LRRK2-WT, LRRK2-G2019S, or LRRK2-R1441C mutant constructs and GFP-tagged v-SNARES or GFP as mock, as indicated. Forty-eight h after transfection, lysates were subjected to co-immunoprecipitation using GFP antibody and processed for SDS-PAGE and western blot analysis. Inputs represent 3% of the cell extract used for immunoprecipitation. Membranes were cut to allow independent incubations and immunoblotted with LRRK2 antibody in the upper part and GFP antibody in the bottom part.

(B, D, F, and H) Quantification of co-immunoprecipitation (co-immunoprecipitated/input signal ratio; see STAR Methods for details) was estimated by densitometry analysis.

(I) *In vitro* pull-down was performed with indicated GST-tagged proteins and purified WT LRRK2 protein. Input (3% of total reaction) and pull-down were submitted to SDS-PAGE and immunoblotted with LRRK2 antibody. Amount of GST proteins present in each reaction is detected using Ponceau staining.

(J) Quantification of pull-down (pulled-down LRRK2/Ponceau signal).

In each panel, mean (colored triangles) and SEM from 3 independent experiments are displayed. One-way ANOVA with Tukey's multiple-comparison test is labeled on graphs. *p < 0.05, **p < 0.01, and ***p < 0.001; ns, not significant.

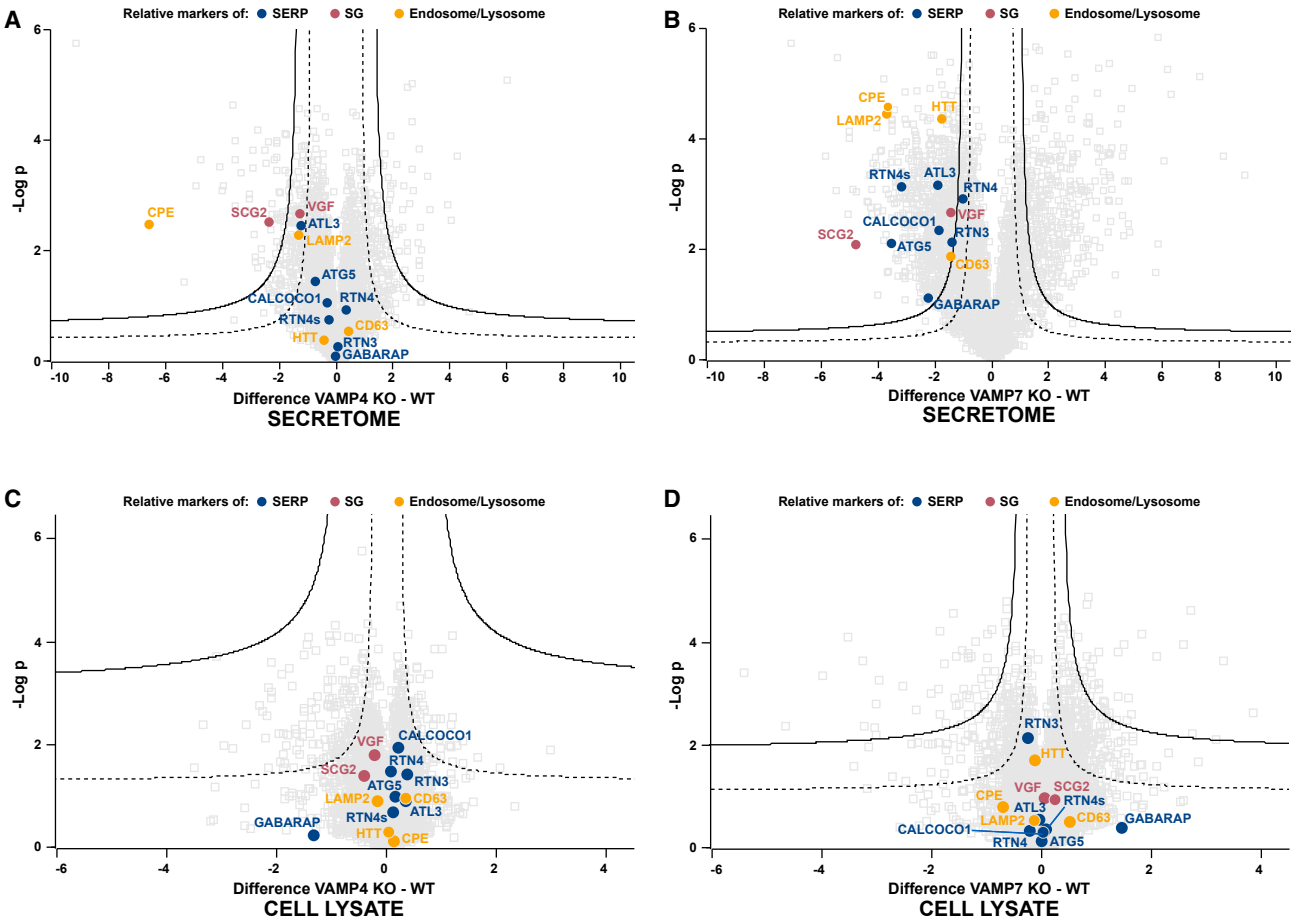

Figure 2. Secretomics and proteomics of WT, VAMP4, and VAMP7 KO PC12 cells

(A–D) Volcano plots showing the secretome (A and B) and proteome of the extracted proteins (C and D) significantly enriched in WT versus VAMP4 KO (A and C) and WT versus VAMP7 KO (B and D). Dashed and plain black lines denote the statistical significance boundary: q values of 0.05 and 0.01, respectively. Proteins of interest are highlighted with colors depending on their group identity (SERP, secretory reticulophagy protein; SG, secretogranin).

We then checked the subcellular localization of LRRK2 WT and mutants compared with VAMP4 and VAMP7. LRRK2 WT and mutant expression confirmed already published localization in HEK293T cells showing diffuse staining for WT and G2019S mutant and the appearance of perinuclear filamentous structures for R14411C mutant[37,38] (Figure S1H). We often observed a tendency of accumulating VAMP4+ membranes within these structures generated by R1441C mutant, as further suggested by a higher Pearson's coefficient (Figure S1I). These results suggested that LRRK2 and VAMP4 interaction might translate into a functional association in the perinuclear region.

Secretion of potential PD biomarker VGF relies on VAMP4 and VAMP7

The results mentioned so far suggested that LRRK2 could play a role in post-Golgi vesicular trafficking via its interaction with VAMP4 and VAMP7. Recent work suggested that LRRK2 regulates retrograde transport to the GA,[23] a route that involves VAMP4 but not VAMP7.[26] Both VAMP4 and VAMP7 play a role in exocytosis, particularly in neurons.[22,27,28] Thus, we asked if VAMP4 and VAMP7 could both be involved in the secretion of identical cargoes. To this end, we used PC12 cells,[39] a classic model to investigate PD mechanisms.[40] We conducted proteomics on cell lysates and secretomics on culture media of NGF-differentiated VAMP4 KO (see Figures S2A and S2B for validation of KO cell lines) and VAMP7 KO[22] PC12 cells. After NGF treatment, cells were cultured without serum for 16 h to avoid albumins and other seric proteins in the secretome. The collection of media was carried out as previously described, followed by cell lysis.[22] Three independent biological and technical experiments were carried out and analyzed using mass spectrometry for cell lysates and corresponding culture media. We plotted the combined score of Gene Ontology (GO) categories that were most affected in VAMP4 KO and VAMP7 KO cell lysates and secretomes (Figures S2C and S2D). This global analysis did not yield obvious common classes of proteins that would be defective in both KO lines. We then restricted the analysis to proteins that were commonly affected by both KOs. The classes of proteins downregulated in both secretomes were related to ribosomes and small nuclear ribonucleoproteins (snRNPs), and

the top classes upregulated in both KOs were related to lysosomal lumen proteins (Figure S2D). The effect of these KOs on ribosomal and snRNP secretion is consistent with our previous findings on secretory reticulophagy,[22] the release of RNA-binding proteins by late endosomal secretion,[41] the accumulation of ribosome-related proteins, and depletion of lysosomal proteins in VAMP4 KO neurons.[28] In the absence of VAMP7, lysosomal lumen proteins might be released in greater amount because they traffic via early endosomes.[42]

We then searched for specific markers of secretion, particularly related to late endosomal secretion, which would be similarly affected by both KOs (Figures 2A and 2B). We first observed that we had reproduced the effect of VAMP7 KO on secretory reticulophagy markers (ATL3, CALCOCO1, RTN3, RTN4 long and short forms, ATG5, and GABARAP; Figure 2B, blue circles in volcano plots[22]). In the VAMP4 KO secretomes (Figure 2A), secretory reticulophagy proteins, referred as SERP,[43] such as ATL3 were significantly decreased, but the effect was not as extensive as in VAMP7 KO (Figure 2B). Several proteins related to the endolysosomal system (yellow circles) were decreased in the VAMP4 KO (CPE and LAMP2) and in the VAMP7 KO (CPE, LAMP2, and CD63) clearly suggesting a defect in late endosomal secretion in both KO (Figures 2A and 2B) and potentially a defect in transport to late endosomes[42] of these transmembrane proteins. In this category, the VAMP7 KO secretome (Figure 2B) was particularly depleted in HTT, which was shown to be released by late endosomes,[44] but this was not the case for the VAMP4 KO secretome (Figure 2A). Two secretogranins, SCG2 and, more significantly and interesting for the purpose of this study, VGF, were significantly decreased in both KOs (Figures 2A and 2B, pink circles). Indeed, VGF is a SG recently identified as a potential PD biomarker.[31,33] None of these proteins appeared significantly affected in cell lysates of both KOs (Figures 2C and 2D). VGF thus appeared as the clearest and most interesting protein in relation with PD, the secretion of which was downregulated in both VAMP4 and VAMP7 KOs.

VAMP4 and VAMP7 regulate the secretion of VGF

We then went on to characterize more precisely secretion of VGF in our KO cells. To this end, we performed western blotting on cell lysates and secreted fractions from WT, VAMP4, VAMP7 KOs, and VAMP2 KO PC12 cells as control. Total protein content of secreted fractions was obtained by acetone precipitation as previously described.[22] We also extracted large dense (at 15,000 × *g*) and small light (at 200,000 × *g*) extracellular vesicles by pelleting the cell medium, previously precleared of debris at 2,000 × *g*. To get insight of the exact size of particles secreted in large and small EVs, we used dynamic light scattering, and we detected two different picks at around 430 nm for EVs pelleting at 15,000 × *g* and 140 nm for EVs pelleting at 200,000 × *g* (Figure S3A). Small EVs were further characterized using western blot; we found that those vesicles are positive for conventional exosome markers HSC70 and TSG101[45] (Figure S3B).

We then blotted for VGF using a monoclonal antibody directed against amino acids (aa) 159–223, a region in the moiety of the pro-VGF that encompasses fragments of VGF that are proteolyzed along the secretory pathway. As already described,[46] we detected three main bands: 80 kDa corresponding to pro-VGF and 78 and 68 kDa, which correspond to large VGF fragments (Figure 3A). We further quantified the secreted VGF as a fraction of the cellular content to compare fractional release among cells of different genotypes (Figure 3B), and this confirmed our mass spectrometry results (Figure 2). The loss of VAMP4 and VAMP7 both led to a decreased pro-VGF release compared with the WT secreted fraction. The cellular content of pro-VGF in the VAMP4 KO but not in the VAMP7 KO appeared significantly decreased compared with WT PC12 (Figure 3B). We did not observe significant differences in the total pool of released pro-VGF between in VAMP2 KO cells. VGF has recently been observed to be decreased in the urinary proteome of PD patients and G2019S mutation carriers,[33] and interestingly, the form identified in this later study contains peptides that make it possible to hypothesize that it might correspond also to pro-VGF. The secretion of pro-VGF was significantly decreased in VAMP7 KO cells, in both large and small EVs, suggesting that VAMP7 is required for the late endosomal secretion of the pro-peptide. Conversely, we were not able to detect a similar decrease in EVs of VAMP4 KO cells as recapitulated by the total released fractions. Large EVs of VAMP2 KO cells showed increased secretion of pro-VGF, probably due to impaired trafficking toward secretory granules (Figure 3B).

We then compared the release in EVs of WT, VAMP7, and autophagy-null ATG5 KO PC12 cells. ATG5 KO cells released more pro-VGF in small EVs compared with WT and VAMP7 KO PC12 cells (Figures 3C and 3D). These experiments further confirmed our previous findings regarding reduced secretion of RTN3 in VAMP7 KO cells,[22] at both 15,000 × *g* and 200,000 × *g*. These data further demonstrate that VAMP7 KO cells are defective in late endosomal secretion which mediates the release of EVs.

Altogether, our results are consistent with the conclusions that (1) a fraction of unprocessed pro-VGF is released as seen in WT PC12 cells, (2) VAMP4 KO results in decreased release of pro-VGF because of impaired expression, and (3) pro-VGF release is decreased in VAMP7 KO because of a more direct effect on its secretion, as suggested by the significant decreased in large and small EVs, without a significant effect on its expression.

To assess the possible role of LRRK2 in VGF secretion, we chose to exogenously express VGF and WT or PD-associated mutants of LRRK2 in HEK293T, cells in which these proteins are expressed at extremely low levels (https://www.proteinatlas.org/ENSG00000128564-VGF/cell+line and https://www.proteinatlas.org/ENSG00000188906-LRRK2/cell+line). We followed the same procedure as the one used for PC12 cells to analyze cell lysates and total secreted media. We found that expression of GFP-LRRK2-WT, GFP-LRRK2-G2019S, and GFP-LRRK2-R1441C all increased the amount of pro-VGF in cell lysate and decreased the secreted fraction recovered in the cell medium in relation to the total content (Figures 3E and 3F). We also examined the subcellular localization of exogenous VGF in those same cells co-transfected with GFP-LRRK2-WT/GFP-LRRK2-G2019S/GFP-LRRK2-R1441C and stained for endogenous VAMP4 or VAMP7 (Figure S3C). The expression of VGF in HEK293T cells resulted in dot-like staining reminiscent of secretory vesicles. VGF further appeared to a low extent in VAMP4+ and VAMP7+ compartments upon expression of LRRK2 WT, G2019S, and more particularly R1441C mutants. Interestingly,

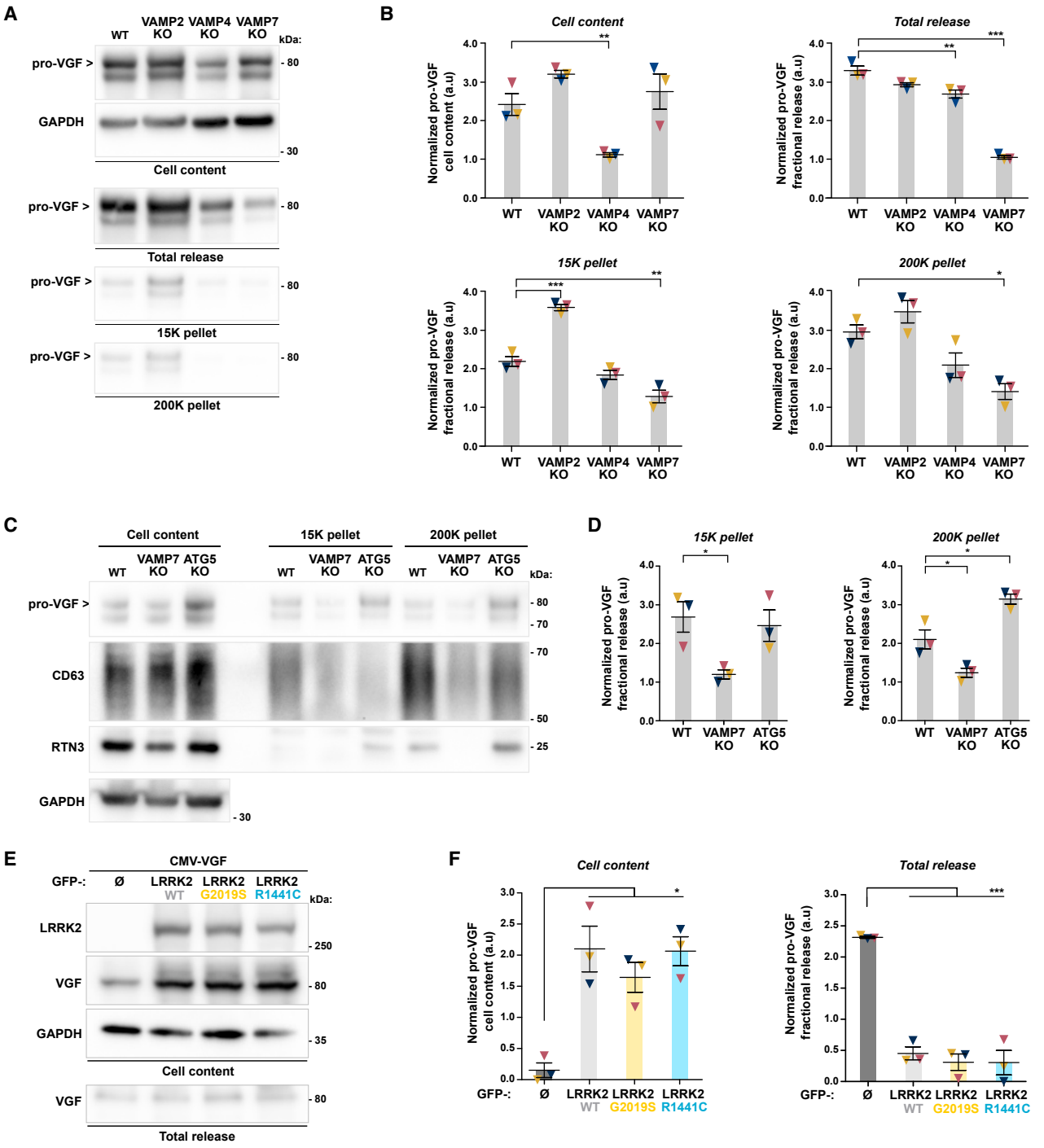

Figure 3. Validation of VAMP4 and VAMP7 KO secretomes by western blot

(A, C, and E) WT, VAMP2 KO, VAMP4 KO, and VAMP7 KO PC12 were differentiated with NGF for one week (A and C). (E) HEK293T cells were transfected with indicated constructs. Equal amounts of cell lysate proteins (~15 μg) and volumes of secreted fractions ("total release," "15K pellet," and "200K pellet") corresponding to equal cell lysate protein concentration were processed for SDS-PAGE and western blot analysis. Membranes were probed with indicated antibodies.

(B, D, and F) Cell content (cell lysates/GAPDH), fractional release for total and 15K/200K pellet (secreted fraction/cell lysate) of pro-VGF was estimated by densitometry analysis of the corresponding bands from three independent experiments.

Mean (colored triangles) and SEM of three independent experiments are displayed. One-way ANOVA with Tukey's multiple-comparison test is labeled on graphs. *$p < 0.05$, **$p < 0.01$, and ***$p < 0.001$; ns, not significant.

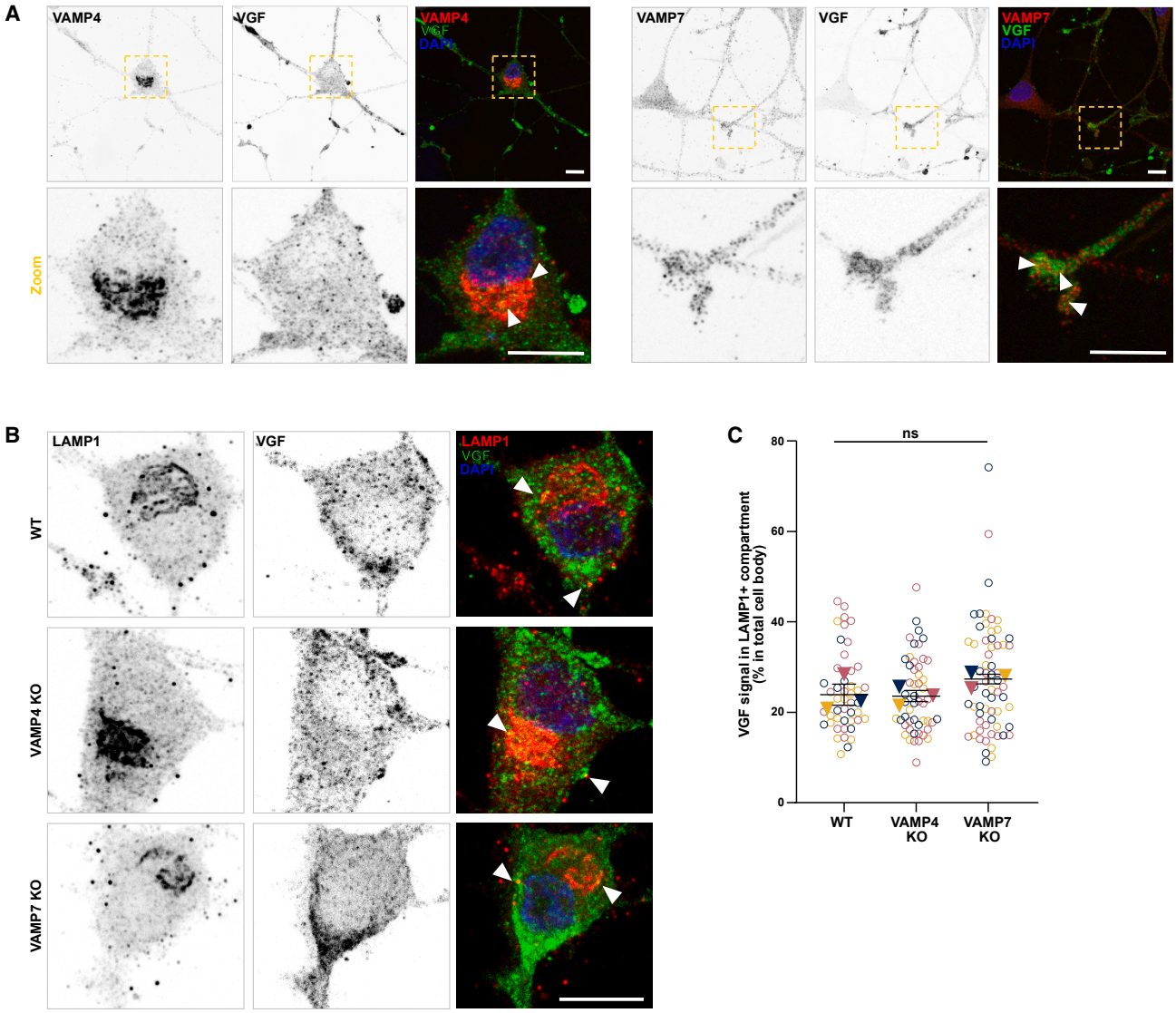

Figure 4. A pool of VGF localizes in VAMP4, VAMP7, and LAMP1 compartments

(A) WT PC12 cells were differentiated with NGF for one week and processed for immunocytochemistry. The cells were stained for endogenous VAMP4 (left, red) or VAMP7 (right, red) and VGF (green). Magnifications of dash-delimited regions are displayed in the bottom row. Projections of confocal microscopy optical section are shown. Arrowheads indicate red-green co-stained structures. Scale bar, 10 μm.

(B) WT, VAMP4 KO, and VAMP7 KO PC12 were differentiated with NGF for 1 week and processed for immunocytochemistry. Whole projections of confocal microscopy optical section are shown. Cells were stained for LAMP1 (red) and VGF (green). Arrowheads indicate red-green co-stained structures. Scale bar, 10 μm.

(C) Quantification of VGF signal detected in LAMP1+ vesicles in cell body area (% of total VGF signal in cell body). One-way ANOVA with Tukey's multiple-comparison test is displayed on graph. ns, not significant.

we observed accumulation of VGF in perinuclear regions, where VAMP4 and VAMP7 also localized, in cells expressing GFP-LRRK2-G2019S and GFP-LRRK2-R1441C.

Role of VAMP4 and VAMP7 in VGF trafficking

We went on to investigate the localization of VGF in VAMP4+ and VAMP7+ intracellular membrane compartments in WT NGF-differentiated PC12 cells. Previous studies showed that VGF is targeted to secretory granules, similarly to other granins.[46] We stained NGF-differentiated WT PC12 cells for endogenous VGF, VAMP4, or VAMP7 (Figure 4A). VAMP4 localized in the perinuclear region of cell bodies and was also present in neurites to a lesser degree. VAMP7 localized mostly in neurite terminals. Such partial enrichment would be compatible with the presence of only a pool of VGF in VAMP4+ and VAMP7+ compartments. Ascertaining whether that pool would correspond to unprocessed alone or in combination with processed VGF was not technically feasible with available tools.

We previously showed that pro-VGF expression was downregulated in VAMP4 KO (Figures 2A and 2B) and that VAMP7 mediates late endosomal and lysosomal secretion[22,47] (for secretomics analysis showing the effect on CD63 and LAMP2, see Figure 2B). This led us to characterize the potential presence of VGF in late endosomes and lysosomes in WT vs. VAMP4 and VAMP7 KO PC12 cells.

We checked the localization of VGF in LAMP1-positive vesicles in PC12 cell bodies only because VAMP7 KO cells did not grow long neurites as previously described.[22] We found that in both WT and KO cells, a subset of VGF (~24%) could be detected as associated with late compartments (Figure 4B). As shown by Pearson correlation analysis, no difference was detected when comparing WT and VAMP4 or VAMP7 KO cells (Figure 4C).

When LAMP1+ vesicles were distinguished depending on their clustering (Figures S4A and S4B), to discriminate "clustered" perinuclear degradative endosomes and "dispersed" peripheral secretory ones,[14,48] both VAMP4 and VAMP7 KO cells displayed lower VGF localization together with dispersed LAMP1+ vesicles compared with WT PC12 cells. In the case of clustered LAMP1+ vesicles, VGF displayed the same degree of localization together with LAMP1+ lysosomes in WT and both KO PC12 cells.

In conclusion, detailed analysis of VGF localization and secretion in both VAMP4 and VAMP7 KO cells validated secretomics data and demonstrated that both VAMPs play a role in VGF trafficking and secretion. Altogether, our results suggest that a pool of VGF, potentially the pro-peptide, is trafficked together with LAMP1 in a VAMP4- and VAMP7-dependent manner for late endosomal secretion and that LRRK2 affects this process.

VGF is trafficked via VAMP4 and VAMP7 in a LRRK2-dependent manner

To identify more precisely the stage in secretion that LRRK2 might regulate, we took advantage of the retention using selective hooks system.[34] This streptavidin/biotin-based assay allows the retention of proteins of interest in the ER and synchronizes their release in the secretory pathway upon addition of biotin in the cell media (Figure 5A). We generated RUSH-VGF-mCherry and studied its trafficking, which we described and characterized to be transported from the ER to the perinuclear region where the GA marker N-acetylglucosamine transferase (NAGT)[49] is localized and targeted to the plasma membrane in HEK293T cells within 80 min after addition of biotin (Video S1; Figure 5B).[34,50] We showed that pro-VGF is still detectable 60 min after the addition of biotin (Figure 5C) and we investigated the precise compartments by which VGF follows the secretory pathway. We found that 15 min after the addition of biotin, VGF is partially found in perinuclear VAMP4+ compartments, and after 60 min some of it is found in compartments that are positive for both CD63 and VAMP7 (Figure 5D). These results suggested that VAMP4 and VAMP7 could regulate the VGF route from the ER to the plasma membrane.

We studied the transport of VGF from the ER to the PM in control conditions and in GFP-LRRK2-WT, GFP-LRRK2-G2019, and GFP-LRRK2-R1441C expressing cells. The mCherry tag allowed the study of VGF trafficking and GA localization was confirmed by GM130 co-staining following fixation. To efficiently study the intracellular trafficking of VGF, HEK239T cells were analyzed using immunofluorescence at different time points after addition of biotin, as described in STAR Methods. All conditions displayed the expected route of VGF from the ER to the GM130+ GA region to the PM. Before biotin addition, VGF consistently localized in the ER (Video S1; Figure 5B). In control GFP-expressing cells, the cargo was correctly transported from the ER, trafficked to the GA region, and released in vesicles on the way to the PM within 60 min after biotin addition. In the case of LRRK2-expressing cells, the transport of VGF was delayed, resulting in accumulation in the GA region and consequent inhibition of delivery to the PM (Figures 6A and 6B). As shown in Figure 6B (and three-dimensional [3D] visualization in Video S2), VGF is still retained into the GA region 60 min after biotin addition, whereas in GFP control condition, it appears to be already in the cell periphery. All conditions with LRRK2 expression, WT and mutants, appear to significantly delay the transport of VGF out of the perinuclear region, but the largest difference was observed with the PD-associated LRRK2 mutants R1441C compared with the WT (Figure 6C).

We also studied the transport of TNF-α, a secreted inflammatory biomarker of PD[51] and well characterized cargo used in the RUSH assay,[52] finding that the latest is also trafficked in part in VAMP4+ and VAMP7+ structures in cells expressing LRRK2 (Figure S5). We confirmed a similar delay in the trafficking of TNF-α because of WT and PD-associated LRRK2 mutants (Figure S6). All conditions at 20 min after biotin addition, TNF-α was found at an equivalent level at the perinuclear region, meaning that the defect due to LRRK2 WT and mutant expression was likely in the cell center. RUSH assay experiments thus allow to conclude that VGF is in part transported via VAMP4+ and VAMP7+ compartments and that LRRK2 expression, particularly R1441C, delay transport from the cell center to the cell periphery, where secretion occurs.

VGF trafficking is impaired in primary neurons

We went on to confirm our observation in cells which could be a closer model to PD pathology. We used rat DIV8 (day *in vitro* 8) primary hippocampal neurons co-transfected with WT or PD-associated R1441C LRRK2 mutant together with VGF. We used RFP as negative control and RFP-Longin as a positive control (Figures 7A and 7B). Indeed, expression of the Longin domain of VAMP7 was shown both in cultured cells and *in vivo* in the brain to impair VAMP7-dependent late endosomal secretion[53–55] and secretory reticulophagy.[22] We found that expression of the Longin domain prevented the proper peripheral distribution of VGF in neurites resulting in accumulation at the level of the soma. The expression of both WT and LRRK2 R1441C mutant resulted in an even stronger significant accumulation of VGF at the soma level. These data confirmed that the trafficking from the cell center to the periphery of VGF is a LRRK2-dependent mechanism and that VAMP7 participates to this process in hippocampal neurons.

DISCUSSION

Growing evidence links disruption of the endolysosomal system to PD. In particular, LRRK2 mutations were shown to lead to

CellPress
OPEN ACCESS

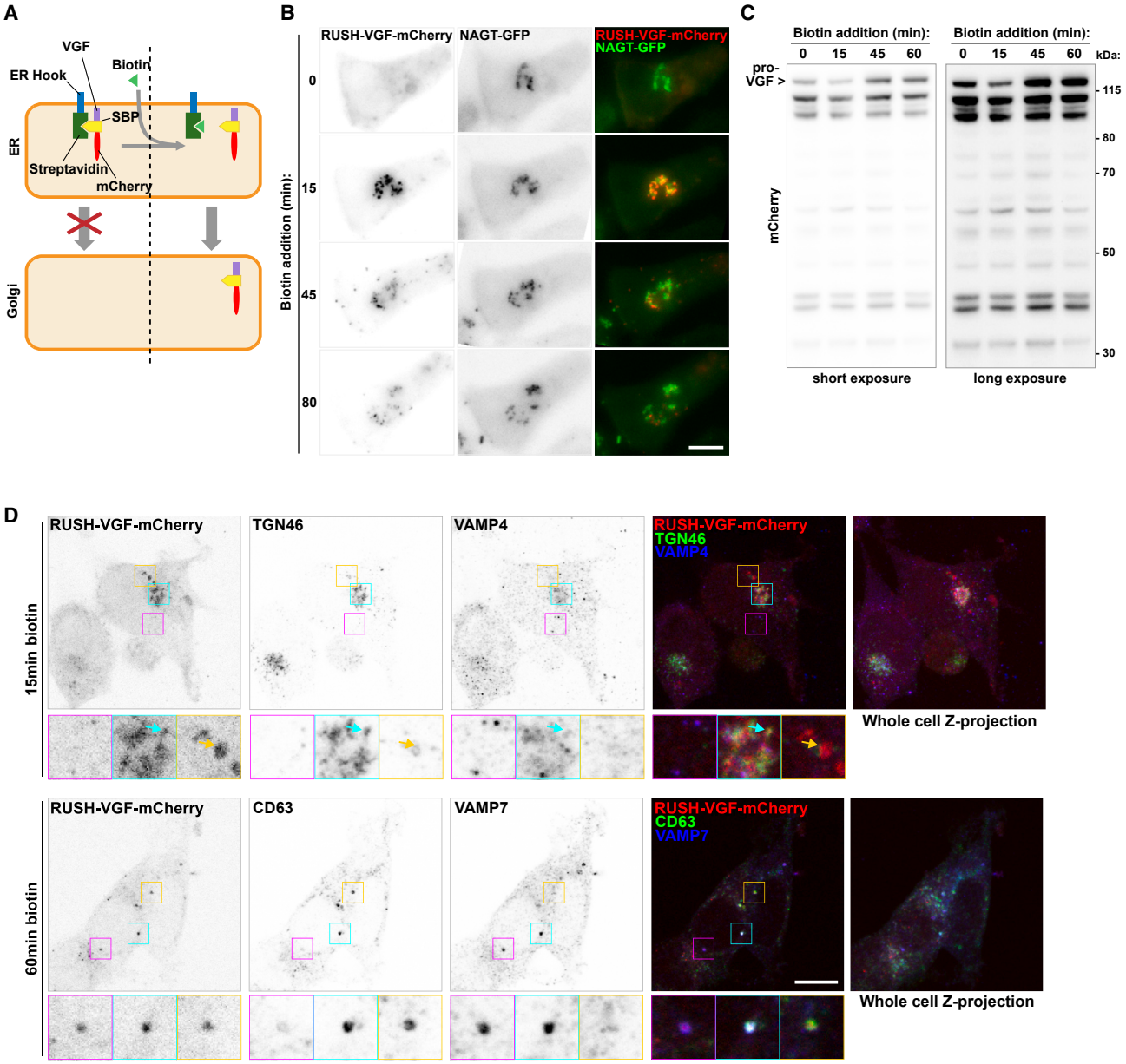

Figure 5. VGF follows ER to PM route via VAMP4 and VAMP7 compartments

(A) Schematic representation of RUSH-VGF-mCherry trafficking upon biotin addition. The RUSH system is based on the expression of two fusion proteins: (1) an ER retention hook (Lys-Asp-Glu-Leu; KDEL) fused to core streptavidin and (2) a cargo protein fused to SBP (streptavidin-binding protein) and mCherry. Because of the high-affinity SBP/streptavidin interaction, the VGF cargo is retained in the ER. Addition of biotin to the cell medium triggers a synchronous release of the cargo from the ER and its transport across the GA to the cell surface, which can be monitored via mCherry tag.

(B) Still images from Video S1. Trafficking of RUSH-VGF-mCherry co-expressed in HEK293T cells with GA marker (N-acetylglucosaminetransferase [NAGT]) upon biotin addition: t = 0 min (addition of biotin), at the ER; t = 15 min at the GA; t = 45 min, partially still at the GA and post-Golgi vesicles; t = 80 min, mainly targeted at the PM.

(C) HEK293T transfected with RUSH-VGF-mCherry were submitted to biotin chase for the indicated times and lysed. Equal amounts of cell lysate proteins were processed for SDS-PAGE and mCherry immunoblot (short and long ECL exposures are shown). Note the presence of multiples bands below pro-VGF (80 kDa) that correspond to C-terminally mCherry-tagged cleaved VGF peptides.

(D) RUSH-VGF-mCherry trafficking in HEK293T cells. After 15 min (top) and 60 min (bottom) of biotin incubation, cells were immunostained for mCherry (red), TGN marker TGN46 (green), and VAMP4 (blue) 15 min after biotin addition (top panels) and for CD63 (green) and VAMP7 (blue) 60 min after biotin addition (bottom panels). Projections of confocal microscopy optical sections of less than 1 μm are shown (black and white and three color micrographs). Whole Z projections of confocal microscopy optical sections are shown for each condition in the right panels as indicated. Bottom rows show magnifications of the colored boxed areas depicting co-stained structures further indicated by arrows. Scale bar, 10 μm.

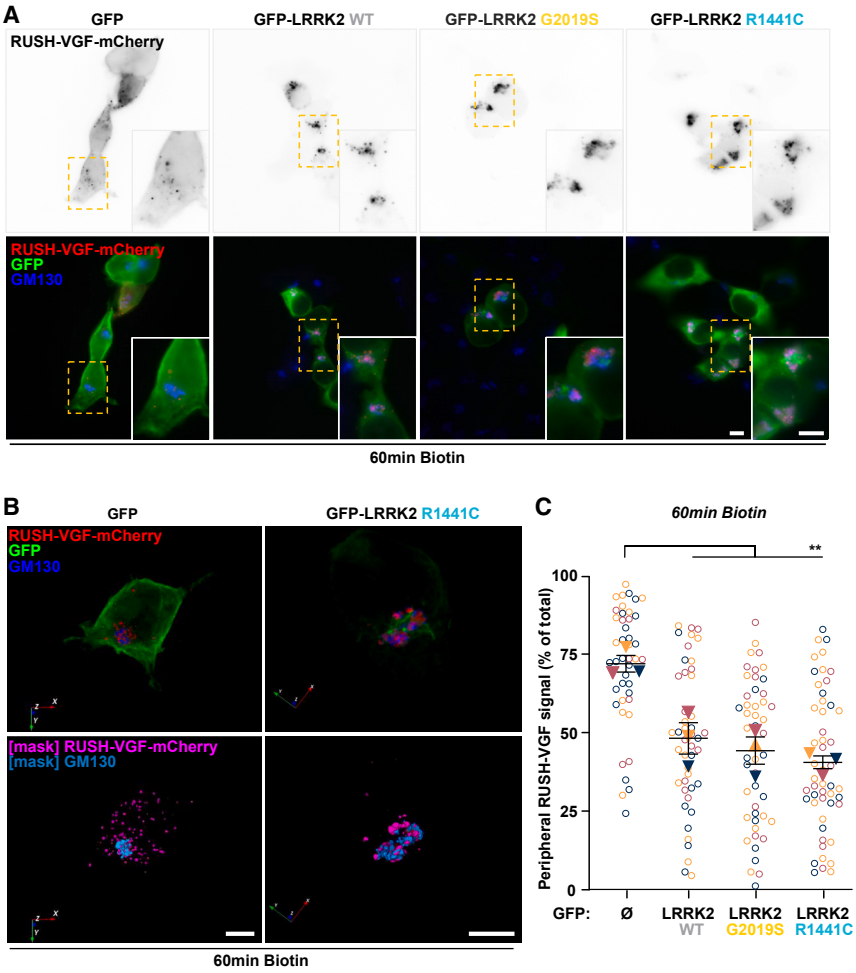

Figure 6. LRRK2 expression retards VGF secretion with retention in the Golgi apparatus region

(A) Synchronized transport of RUSH-VGF-mCherry in HEK293T cells. Cells were co-transfected with GFP, GFP-WT, or G2019S or R1441C LRRK2 mutants and RUSH-VGF-mCherry. Biotin was added to release RUSH-VGF-mCherry from the ER and 60 min after biotin addition, and cells were fixed and stained with GFP and GM130 antibodies to detect transfected cells and GA, respectively. Wide-field fluorescent images are shown. Note the signal overlay of GM130 with RUSH-VGF-mCherry in LRRK2-expressing cells, compared with GFP-expressing control cells (dashed boxed regions and insets).

(B) Representative example of 3D confocal Zstack of HEK293T cells expressing RUSH-VGF-mCherry and GFP control condition (left) or GFP-LRRK2-R1441C (right) 60 min after biotin addition. Corresponding 3D masks of RUSH-VGF-mCherry and GM130 used for quantification are depicted (bottom panels). See 3D visualization (Video S2) for a representative example of all tested LRRK2 constructs.

(C) Quantification of the RUSH-VGF-mCherry signal present at cell periphery (outside GM130 mask) over total signal, 60 min after biotin addition. Horizontal lines show mean ± SEM, while colored circles and triangles represent values of individual cells and mean of 3 independent experiments, respectively. One-way ANOVA with Tukey's multiple-comparison test was performed from each triplicate mean values. **p < 0.01. Scale bar, 10 μm.

dysfunction of the endolysosomal membrane trafficking.[56,57] Here we investigated the effect of expressing WT and PD mutants of LRRK2 on v-SNARE-dependent trafficking and secretion by using biochemical, mass spectrometry, imaging, and membrane trafficking functional assays. We found that LRRK2 very efficiently interacted with the endosomal v-SNAREs VAMP4 and VAMP7, the R1441C mutant of LRRK2 being the most efficient interactor of VAMP4. We showed that VAMP4 and VAMP7 KO cells' neuronal secretomes were both depleted in pro-VGF, and further analysis confirmed that the pro-peptide is decreased in both KO cell lines in the total secreted fraction as well as EVs. LRRK2 and its mutants, particularly R1441C, further affected the secretion of pro-VGF and resulted in its accumulation in cells. We further found that expression of WT and mutant LRRK2 delayed the exit of VGF from the cell center both in non-neuronal cells and hippocampal neurons.

LRRK1, a LRRK2 paralog, phosphorylates CLIP-170 and interacts with dynein molecular motor to mediate retrograde transport of endosomes on microtubules.[58] Cells lacking LRRK1 show peripheral accumulation of VAMP7.[14] Human G2019S LRRK2 mutant expressed in LRRK loss-of-function background promotes retrograde transport in fly neurons.[59] This mutant particularly perturbs the transport of axonal autophagosomes.[60] In addition, reduced LRRK2 kinase activity was shown to increase anterograde axonal transport of α-synuclein.[61] LRRK2 further regulates retrograde transport to the GA via its interaction with Golgi-associated retrograde protein complex.[23] The structure of the catalytic half of LRRK2 and the atomic model of microtubule-associated LRRK2 suggested a role as a roadblock for motor proteins, both anterograde kinesins and retrograde dynein.[62] When considering our finding of a LRRK2 interaction with VAMP4 and VAMP7 and retention of secreted peptides such as VGF and TNF-α in the cell center, a reasonable hypothesis could be that LRRK2 plays a checkpoint role in the secretory pathway. The principal fate of pro-VGF is to be processed by Golgi enzymes such as pro-convertases to generate peptides which are released by secretory granules and such secretion is VAMP2 dependent[63] (Figure 7C, route 1). Indeed, here we found that VAMP2 KO PC12 cells tended to accumulate the pro-peptide. VAMP4 mediates retrograde transport from endosomes to the GA in non-neuronal cells[26] and retrograde transport of synaptic vesicles proteins from endosomes to endolysosomes in nerve terminals.[28] VAMP4 localizes both to the GA and endosomes.[26] As shown in our study, cells lacking VAMP4 are expressing and releasing less pro-VGF compared with WT cells. It would thus be tempting to

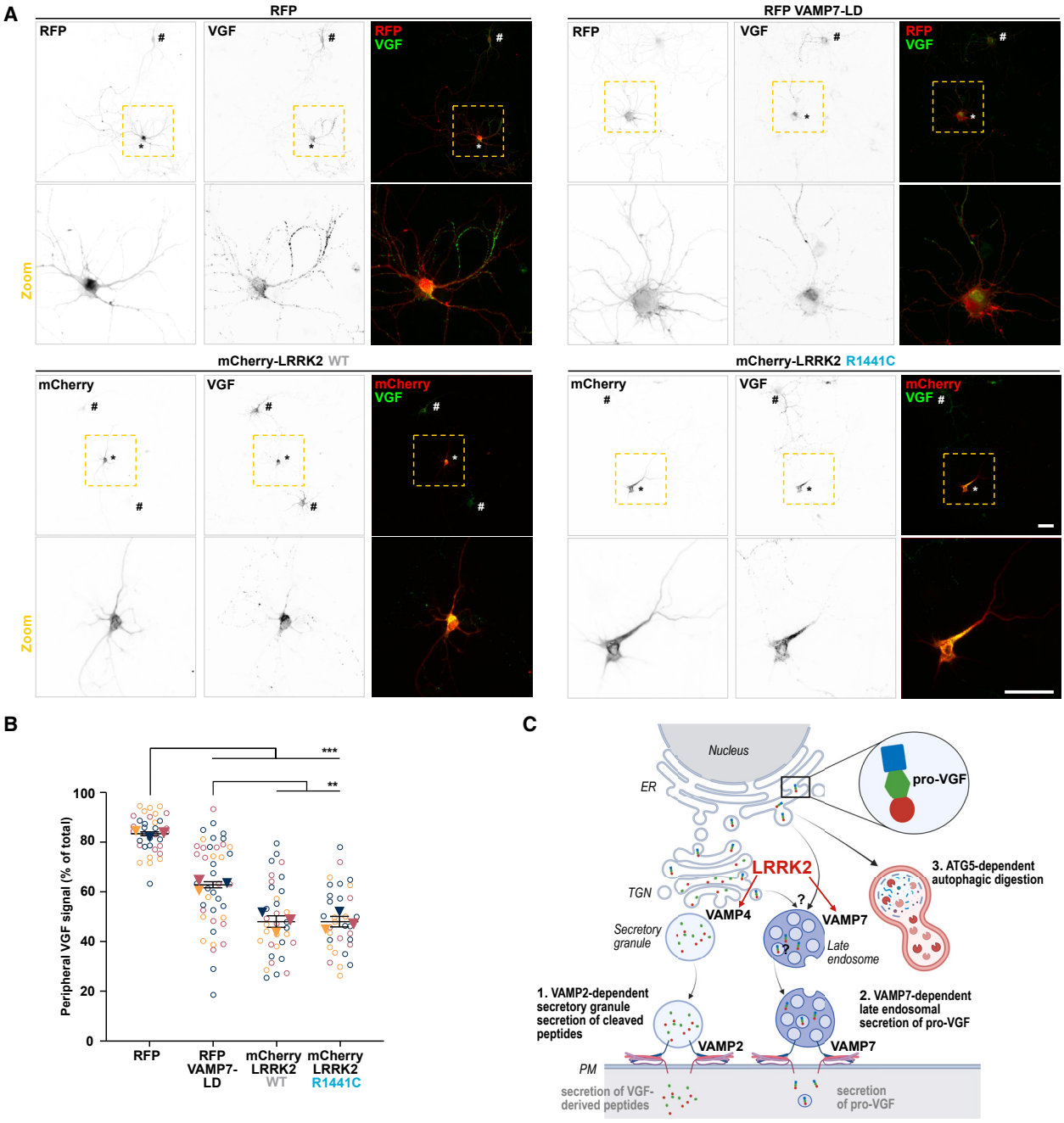

Figure 7. Defect of VGF transport to neurites in VAMP7-LD and LRRK2-expressing primary neurons and hypothetical model

(A) DIV6 primary hippocampal neurons were transfected with CMV-VGF and RFP, RFP-VAMP7-LD, mCherry-LRRK2 WT, or mCherry-LRRK2 R1441C, fixed at DIV8, and stained with mCherry and VGF antibodies. Wide-field fluorescent images are shown. Pound sign and asterisk correspond to RFP− and RFP+ cell soma, respectively.

(B) Quantification of peripheral (excluded from soma) over total VGF signal ratio. Horizontal lines show mean ± SEM of 3 color-coded independent experiments, while circles and triangles represent values of individual cells and mean of each experiment, respectively. One-way ANOVA with Tukey's multiple-comparison test was performed from each triplicate mean values. **$p < 0.01$ and ***$p < 0.001$. Scale bar, 50 μm.

(C) Hypothetical model of the routes of pro-VGF trafficking unraveled in this study: (1) VAMP2-dependent regulated secretion of VGF peptides, (2) VAMP7-dependent late endosomal secretion of pro-VGF, and (3) ATG5-dependent autophagic degradation of pro-VGF. LRRK2 interaction with VAMP4 and VAMP7 would function as a checkpoint for the secretory pathway in the cell center.

hypothesize that LRRK2 might recruit VAMP4 in retrograde transport[23,26] of pro-VGF back to the GA as a way to recover the pro-peptide and put it back in the route 1 (Figure 7C). This would be in good agreement with previous findings suggesting a role of VAMP4 in secretory granule maturation[64] and insulin trafficking.[65] In the absence of VAMP4, more pro-VGF might thus be degraded by autophagy (Figure 7C, route 3) or other mechanisms. VAMP7 was shown to mediate late endosomal and lysosomal secretion[66] and transport from the TGN to late endosomes.[42] Secretory lysosomes are located in the cell periphery and their exocytosis is involved in plasma membrane repair[67] and ATP release.[47,68] According to work in the Grinstein lab,[69] juxtanuclear lysosomes are more acidic and have higher cathepsin L activity than peripheral lysosomes. Central lysosomes and late endosomes are clustered, more acidic, more degradative, whereas the peripheral ones are more dispersed, and less acidic as recently reviewed.[70] Previous work showed that VAMP7 was associated with secretory lysosomes which are mildly acidic in sensory neurons.[71] Our secretomics is in good agreement with the abovementioned studies, as we found defective secretion of transmembrane late endosomal/lysosomal proteins CPE, LAMP2, and CD63 but not lysosomal luminal proteins which traffic first to early endosomes before being routed to late endosomes.[42] Here, in the absence of VAMP7, cells released less pro-VGF, particularly co-precipitating with EVs, but expression of the peptide was unaffected (Figure 7B, route 3). The fact that expression of pro-VGF level was unaffected in VAMP7 KO cells would speak against a defect in its processing because of mistargeting of pro-convertases. This hypothetical model would position LRRK2 in a similar function as LRRK1 to downregulate availability of VAMP7 for secretion in the cell periphery.[14] In most of our experiments, WT and the mutant LRRK2 behaved somewhat similarly, but the R1441C was the most efficient in interacting with VAMP4 and inhibiting transport of VGF to the cell periphery. In our hands, expression of WT and mutant LRRK2 lead to increased expression of pro-VGF and its decreased secretion when considering fractional release of the peptide (released amount/total expression). The literature and our data thus suggest that the activity of LRRK2 might affect the three routes proposed here (regulated secretion of VGF peptides, late endosomal secretion of pro-VGF, and autophagic degradation of pro-VGF). Further studies are required to connect the GTPase and kinase activity with the new pathways uncovered here.

LRRK2, VAMP4, and VGF have been clearly associated with PD. Here we were able to propose a hypothetical mechanism linking these three genes' products. VGF has been shown to be a biomarker of PD,[31] and particularly of interest in the context of our study, it was found to be decreased in urinary proteome of sporadic PD and LRRK2-G2019S patients.[33] Here we found that VGF is overexpressed when LRRK2 is co-expressed and that autophagy-null cells release more pro-VGF. Again, this is reminiscent of the elimination of mutant insulin by reticulophagy.[72] The processing of pro-peptides, particularly prone to aggregation in the TGN such as a secretogranin[73] like VGF, by autophagy, might thus be an important regulation in which LRRK2 could participate (Figure 7C, route 3). A defect in elimination of the excess of pro-peptide by autophagy would lead, in our hypothetical model (Figure 7C), to more secretion by late endosomes. Several recent studies are revealing the importance of non-cell-autonomous processes that are responsible for the death of dopaminergic neurons in PD.[74] Most of the PD-associated proteins are not uniquely expressed in the substantia nigra pars compacta, where dopaminergic neurons are located, but also in other regions and cell types of the central nervous system. A potential hypothesis is that neurodegeneration in PD is caused by a cell-autonomous mechanism within neurons, amplified by a non-cell-autonomous related to the secretion of factors such as VGF and TNF-α. Alternatively, the secretion of pro-VGF by late endosomes might be merely an indicator of VGF production by healthy neurons and the VGF defects in patients would be only a symptom. In both hypotheses, LRRK2 and VAMP4 could act in concert in such mechanisms. In addition, our finding that part of VGF co-precipitates with EVs might be a reasonable explanation of its presence in body fluids, including urine,[33] because if some VGF was inside EVs, it would be protected from degradation by body fluid proteases. It will now be important to explore the mechanism which allows VGF to go from the brain or neuroendocrine tissues to the blood and urine.

The potential mechanism unraveled here provides new grounds to hypothesize that LRRK2 mutations might modify the environment of dopaminergic neurons and induce long-term effects leading to their death. Our data further suggest that the secretion of pro-peptides by late endosomes might be relevant to PD physio-pathological mechanisms. Future directions should include connecting our findings with the role of LRRK2 in phosphorylating Rab proteins, particularly Rab8,[56] which directly interacts and regulates VAMP7[75] and VGF trafficking with other PD risk factors.

Limitations of the study

We used primarily exogenous expression in cell lines and primary cultured neurons to decipher novel molecular mechanisms related to LRRK2. Further studies should include the use of genomic modifications to introduce tags and mutations in LRRK2 gene.

We have not yet been able to demonstrate whether part of VGF could be inserted inside extracellular vesicles or if the pelleted released fraction of VGF corresponded to aggregated luminal pro-peptide. Further studies are needed to address this question in cultured cells and body fluid EVs.

STAR★METHODS

Detailed methods are provided in the online version of this paper and include the following:

- KEY RESOURCES TABLE
- RESOURCE AVAILABILITY
  - Lead contact
  - Materials availability
  - Data and code availability
- EXPERIMENTAL MODELS AND SUBJECT DETAILS
  - Cell lines
  - Primary culture
- METHOD DETAILS

- CRISPR/Cas9 genetic engineering
- Plasmids
- Protein electrophoresis and Western blot
- Immunoprecipitation
- GST pull-down
- Secretion assay
- Immunofluorescence
- RUSH assay
- Live cell imaging
- Confocal imaging
- Proteomic analysis
- Yeast two-hybrid (Y2H)

● QUANTIFICATION AND STATISTICAL ANALYSIS
- Quantification methods
- Data representation and statistical analyses

SUPPLEMENTAL INFORMATION

Supplemental information can be found online at https://doi.org/10.1016/j.celrep.2023.112221.

ACKNOWLEDGMENTS

We thank all members of the laboratory for their assistance and discussions. We also thank our collaborators in Lille Alessia Sarchione and Antoine Marchand for the scientific discussions. Work in our group was funded by grants from the French National Research Agency (MetDePaDi ANR-16-CE16-0012), Institut National du Cancer (PLBIO 2018-149), Fondation pour la Recherche Médicale (FRM, Labellisation), Fondation de France (00096652), and Fondation Bettencourt Schueller (Coup d'Elan) to T.G. J.S. is supported by the American Lebanese Syrian Associated Charities (ALSAC). We thank the B&B facility staff of the Institute of Psychiatry and Neuroscience of Paris (IPNP) for providing access to their instruments and for their technical help. Imaging was carried out at NeurImag Imaging Core Facility, part of the IPNP, INSERM 1266, and Université de Paris. We thank the staff of NeurImag Imaging Core Facility for their scientific expertise in data acquisition, processing, and analysis.

AUTHOR CONTRIBUTIONS

Conceptualization, F.F., T.G., J.-M.T., and M.-C.C.-H.; Methodology, F.F., S.N., K.R., J.W., P.B., M.E., J.S., S.B., J.-C.R., and C.G.; Investigation, F.F., S.N., A.Z., K.R., A.V., P.B., and S.B.; Data Analysis, F.F., S.N., K.R., P.B., and C.G.; Writing – Original & Revised Draft, F.F., S.N., and T.G.; Funding Acquisition, T.G., J.-M.T., and M.-C.C.-H.; Supervision, T.G.

DECLARATION OF INTERESTS

The authors declare no competing interests.

Received: October 5, 2021
Revised: January 12, 2023
Accepted: February 20, 2023
Published: March 10, 2023

REFERENCES

1. Blauwendraat, C., Nalls, M.A., and Singleton, A.B. (2020). The genetic architecture of Parkinson's disease. Lancet Neurol. *19*, 170–178. https://doi.org/10.1016/S1474-4422(19)30287-X.
2. Funayama, M., Hasegawa, K., Kowa, H., Saito, M., Tsuji, S., and Obata, F. (2002). A new locus for Parkinson's disease (PARK8) maps to chromosome 12p11.2-q13.1. Ann. Neurol. *51*, 296–301. https://doi.org/10.1002/ana.10113.
3. Paisán-Ruíz, C., Jain, S., Evans, E.W., Gilks, W.P., Simón, J., van der Brug, M., López de Munain, A., Aparicio, S., Gil, A.M., Khan, N., et al. (2004). Cloning of the gene containing mutations that cause PARK8-linked Parkinson's disease. Neuron *44*, 595–600. https://doi.org/10.1016/j.neuron.2004.10.023.
4. Biskup, S., Mueller, J.C., Sharma, M., Lichtner, P., Zimprich, A., Berg, D., Wüllner, U., Illig, T., Meitinger, T., and Gasser, T. (2005). Common variants of LRRK2 are not associated with sporadic Parkinson's disease. Ann. Neurol. *58*, 905–908. https://doi.org/10.1002/ana.20664.
5. Greggio, E., and Cookson, M.R. (2009). Leucine-rich repeat kinase 2 mutations and Parkinson's disease: three questions. ASN Neuro *1*, e00002. https://doi.org/10.1042/AN20090007.
6. West, A.B., Moore, D.J., Biskup, S., Bugayenko, A., Smith, W.W., Ross, C.A., Dawson, V.L., and Dawson, T.M. (2005). Parkinson's disease-associated mutations in leucine-rich repeat kinase 2 augment kinase activity. Proc. Natl. Acad. Sci. USA *102*, 16842–16847. https://doi.org/10.1073/pnas.0507360102.
7. Biskup, S., Moore, D.J., Celsi, F., Higashi, S., West, A.B., Andrabi, S.A., Kurkinen, K., Yu, S.-W., Savitt, J.M., Waldvogel, H.J., et al. (2006). Localization of LRRK2 to membranous and vesicular structures in mammalian brain. Ann. Neurol. *60*, 557–569. https://doi.org/10.1002/ana.21019.
8. Bonet-Ponce, L., Beilina, A., Williamson, C.D., Lindberg, E., Kluss, J.H., Saez-Atienzar, S., Landeck, N., Kumaran, R., Mamais, A., Bleck, C.K.E., et al. (2020). LRRK2 mediates tubulation and vesicle sorting from lysosomes. Sci. Adv. *6*, eabb2454. https://doi.org/10.1126/sciadv.abb2454.
9. Wang, X., Wu, Y., Cai, S., Ge, J., Shao, L., and De Camilli, P. (2022). Membrane remodeling properties of the Parkinson's disease protein LRRK2. Preprint at bioRxiv. https://doi.org/10.1101/2022.08.10.503505.
10. Steger, M., Diez, F., Dhekne, H.S., Lis, P., Nirujogi, R.S., Karayel, O., Tonelli, F., Martinez, T.N., Lorentzen, E., Pfeffer, S.R., et al. (2017). Systematic proteomic analysis of LRRK2-mediated Rab GTPase phosphorylation establishes a connection to ciliogenesis. Elife *6*, e31012. https://doi.org/10.7554/eLife.31012.
11. Steger, M., Tonelli, F., Ito, G., Davies, P., Trost, M., Vetter, M., Wachter, S., Lorentzen, E., Duddy, G., Wilson, S., et al. (2016). Phosphoproteomics reveals that Parkinson's disease kinase LRRK2 regulates a subset of Rab GTPases. Elife *5*, e12813. https://doi.org/10.7554/eLife.12813.
12. Civiero, L., Vancraenenbroeck, R., Belluzzi, E., Beilina, A., Lobbestael, E., Reyniers, L., Gao, F., Micetic, I., De Maeyer, M., Bubacco, L., et al. (2012). Biochemical characterization of highly purified leucine-rich repeat kinases 1 and 2 demonstrates formation of homodimers. PLoS One *7*, e43472. https://doi.org/10.1371/journal.pone.0043472.
13. Reyniers, L., Del Giudice, M.G., Civiero, L., Belluzzi, E., Lobbestael, E., Beilina, A., Arrigoni, G., Derua, R., Waelkens, E., Li, Y., et al. (2014). Differential protein-protein interactions of LRRK1 and LRRK2 indicate roles in distinct cellular signaling pathways. J. Neurochem. *131*, 239–250. https://doi.org/10.1111/jnc.12798.
14. Wang, G., Nola, S., Bovio, S., Bun, P., Coppey-Moisan, M., Lafont, F., and Galli, T. (2018). Biomechanical control of lysosomal secretion via the VAMP7 hub: a tug-of-war between VARP and LRRK1. iScience *4*, 127–143. https://doi.org/10.1016/j.isci.2018.05.016.
15. Toyofuku, T., Morimoto, K., Sasawatari, S., and Kumanogoh, A. (2015). Leucine-rich repeat kinase 1 regulates autophagy through turning on TBC1D2-dependent Rab7 inactivation. Mol. Cell Biol. *35*, 3044–3058. https://doi.org/10.1128/MCB.00085-15.
16. Burgo, A., Proux-Gillardeaux, V., Sotirakis, E., Bun, P., Casano, A., Verraes, A., Liem, R.K.H., Formstecher, E., Coppey-Moisan, M., and Galli, T. (2012). A molecular network for the transport of the TI-VAMP/VAMP7 vesicles from cell center to periphery. Dev. Cell *23*, 166–180. https://doi.org/10.1016/j.devcel.2012.04.019.
17. Danglot, L., Chaineau, M., Dahan, M., Gendron, M.-C., Boggetto, N., Perez, F., and Galli, T. (2010). Role of TI-VAMP and CD82 in EGFR cell-surface dynamics and signaling. J. Cell Sci. *123*, 723–735. https://doi.org/10.1242/jcs.062497.

18. Martinez-Arca, S., Proux-Gillardeaux, V., Alberts, P., Louvard, D., and Galli, T. (2003). Ectopic expression of syntaxin 1 in the ER redirects TI-VAMP- and cellubrevin-containing vesicles. J. Cell Sci. *116*, 2805–2816. https://doi.org/10.1242/jcs.00467.

19. Martinez-Arca, S., Coco, S., Mainguy, G., Schenk, U., Alberts, P., Bouillé, P., Mezzina, M., Prochiantz, A., Matteoli, M., Louvard, D., and Galli, T. (2001). A common exocytotic mechanism mediates axonal and dendritic outgrowth. J. Neurosci. *21*, 3830–3838. https://doi.org/10.1523/JNEUROSCI.21-11-03830.2001.

20. Alberts, P., Rudge, R., Hinners, I., Muzerelle, A., Martinez-Arca, S., Irinopoulou, T., Marthiens, V., Tooze, S., Rathjen, F., Gaspar, P., and Galli, T. (2003). Cross talk between tetanus neurotoxin-insensitive vesicle-associated membrane protein-mediated transport and L1-mediated adhesion. Mol. Biol. Cell *14*, 4207–4220. https://doi.org/10.1091/mbc.E03-03-0147.

21. Jeppesen, D.K., Fenix, A.M., Franklin, J.L., Higginbotham, J.N., Zhang, Q., Zimmerman, L.J., Liebler, D.C., Ping, J., Liu, Q., Evans, R., et al. (2019). Reassessment of exosome composition. Cell *177*, 428–445.e18. https://doi.org/10.1016/j.cell.2019.02.029.

22. Wojnacki, J., Nola, S., Bun, P., Cholley, B., Filippini, F., Pressé, M.T., Lipecka, J., Man Lam, S., N'guyen, J., Simon, A., et al. (2020). Role of VAMP7-dependent secretion of reticulon 3 in neurite growth. Cell Rep. *33*, 108536. https://doi.org/10.1016/j.celrep.2020.108536.

23. Beilina, A., Bonet-Ponce, L., Kumaran, R., Kordich, J.J., Ishida, M., Mamais, A., Kaganovich, A., Saez-Atienzar, S., Gershlick, D.C., Roosen, D.A., et al. (2020). The Parkinson's disease protein LRRK2 interacts with the GARP complex to promote retrograde transport to the trans-golgi network. Cell Rep. *31*, 107614. https://doi.org/10.1016/j.celrep.2020.107614.

24. Brown, E.E., Blauwendraat, C., Trinh, J., Rizig, M., Nalls, M.A., Leveille, E., Ruskey, J.A., Jonvik, H., Tan, M.M., Bandres-Ciga, S., et al. (2021). Analysis of DNM3 and VAMP4 as genetic modifiers of LRRK2 Parkinson's disease. Neurobiol. Aging *97*. 148.e17–e24. https://doi.org/10.1016/j.neurobiolaging.2020.07.002.

25. Tran, T.H.T., Zeng, Q., and Hong, W. (2007). VAMP4 cycles from the cell surface to the trans-Golgi network via sorting and recycling endosomes. J. Cell Sci. *120*, 1028–1041. https://doi.org/10.1242/jcs.03387.

26. Mallard, F., Tang, B.L., Galli, T., Tenza, D., Saint-Pol, A., Yue, X., Antony, C., Hong, W., Goud, B., and Johannes, L. (2002). Early/recycling endosomes-to-TGN transport involves two SNARE complexes and a Rab6 isoform. J. Cell Biol. *156*, 653–664. https://doi.org/10.1083/jcb.200110081.

27. Grassi, D., Plonka, F.B., Oksdath, M., Guil, A.N., Sosa, L.J., and Quiroga, S. (2015). Selected SNARE proteins are essential for the polarized membrane insertion of igf-1 receptor and the regulation of initial axonal outgrowth in neurons. Cell Discov. *1*, 15023. https://doi.org/10.1038/celldisc.2015.23.

28. Ivanova, D., Dobson, K.L., Gajbhiye, A., Davenport, E.C., Hacker, D., Ultanir, S.K., Trost, M., and Cousin, M.A. (2021). Control of synaptic vesicle release probability via VAMP4 targeting to endolysosomes. Sci. Adv. *7*, eabf3873. https://doi.org/10.1126/sciadv.abf3873.

29. Racchetti, G., Lorusso, A., Schulte, C., Gavello, D., Carabelli, V., D'Alessandro, R., and Meldolesi, J. (2010). Rapid neurite outgrowth in neurosecretory cells and neurons is sustained by the exocytosis of a cytoplasmic organelle, the enlargeosome. J. Cell Sci. *123*, 165–170. https://doi.org/10.1242/jcs.059634.

30. Martinez-Arca, S., Alberts, P., Zahraoui, A., Louvard, D., and Galli, T. (2000). Role of tetanus neurotoxin insensitive vesicle-associated membrane protein (TI-VAMP) in vesicular transport mediating neurite outgrowth. J. Cell Biol. *149*, 889–900. https://doi.org/10.1083/jcb.149.4.889.

31. Cocco, C., Corda, G., Lisci, C., Noli, B., Carta, M., Brancia, C., Manca, E., Masala, C., Marrosu, F., Solla, P., et al. (2020). VGF peptides as novel biomarkers in Parkinson's disease. Cell Tissue Res. *379*, 93–107. https://doi.org/10.1007/s00441-019-03128-1.

32. Karayel, O., Virreira Winter, S., Padmanabhan, S., Kuras, Y.I., Vu, D.T., Tuncali, I., Merchant, K., Wills, A.-M., Scherzer, C.R., and Mann, M. (2022). Proteome profiling of cerebrospinal fluid reveals biomarker candidates for Parkinson's disease. Cell Rep. Med. *3*, 100661. https://doi.org/10.1016/j.xcrm.2022.100661.

33. Virreira Winter, S., Karayel, O., Strauss, M.T., Padmanabhan, S., Surface, M., Merchant, K., Alcalay, R.N., and Mann, M. (2021). Urinary proteome profiling for stratifying patients with familial Parkinson's disease. EMBO Mol. Med. *13*, e13257. https://doi.org/10.15252/emmm.202013257.

34. Boncompain, G., Divoux, S., Gareil, N., de Forges, H., Lescure, A., Latreche, L., Mercanti, V., Jollivet, F., Raposo, G., and Perez, F. (2012). Synchronization of secretory protein traffic in populations of cells. Nat. Methods *9*, 493–498. https://doi.org/10.1038/nmeth.1928.

35. Yun, H.J., Park, J., Ho, D.H., Kim, H., Kim, C.-H., Oh, H., Ga, I., Seo, H., Chang, S., Son, I., and Seol, W. (2013). LRRK2 phosphorylates Snapin and inhibits interaction of Snapin with SNAP-25. Exp. Mol. Med. *45*, e36. https://doi.org/10.1038/emm.2013.68.

36. Myasnikov, A., Zhu, H., Hixson, P., Xie, B., Yu, K., Pitre, A., Peng, J., and Sun, J. (2021). Structural analysis of the full-length human LRRK2. Cell *184*, 3519–3527.e10. https://doi.org/10.1016/j.cell.2021.05.004.

37. Kett, L.R., Boassa, D., Ho, C.C.-Y., Rideout, H.J., Hu, J., Terada, M., Ellisman, M., and Dauer, W.T. (2012). LRRK2 Parkinson disease mutations enhance its microtubule association. Hum. Mol. Genet. *21*, 890–899. https://doi.org/10.1093/hmg/ddr526.

38. Alegre-Abarrategui, J., Christian, H., Lufino, M.M.P., Mutihac, R., Venda, L.L., Ansorge, O., and Wade-Martins, R. (2009). LRRK2 regulates autophagic activity and localizes to specific membrane microdomains in a novel human genomic reporter cellular model. Hum. Mol. Genet. *18*, 4022–4034. https://doi.org/10.1093/hmg/ddp346.

39. Greene, L.A., and Tischler, A.S. (1976). Establishment of a noradrenergic clonal line of rat adrenal pheochromocytoma cells which respond to nerve growth factor. Proc. Natl. Acad. Sci. USA *73*, 2424–2428. https://doi.org/10.1073/pnas.73.7.2424.

40. Grau, C.M., and Greene, L.A. (2012). Use of PC12 cells and rat superior cervical ganglion sympathetic neurons as models for neuroprotective assays relevant to Parkinson's disease. Methods Mol. Biol. *846*, 201–211. https://doi.org/10.1007/978-1-61779-536-7_18.

41. Leidal, A.M., Huang, H.H., Marsh, T., Solvik, T., Zhang, D., Ye, J., Kai, F., Goldsmith, J., Liu, J.Y., Huang, Y.-H., et al. (2020). The LC3-conjugation machinery specifies the loading of RNA-binding proteins into extracellular vesicles. Nat. Cell Biol. *22*, 187–199. https://doi.org/10.1038/s41556-019-0450-y.

42. Pols, M.S., van Meel, E., Oorschot, V., ten Brink, C., Fukuda, M., Swetha, M.G., Mayor, S., and Klumperman, J. (2013). hVps41 and VAMP7 function in direct TGN to late endosome transport of lysosomal membrane proteins. Nat. Commun. *4*, 1361. https://doi.org/10.1038/ncomms2360.

43. Vats, S., and Galli, T. (2021). Introducing secretory reticulophagy/ER-phagy (SERP), a VAMP7-dependent pathway involved in neurite growth. Autophagy *17*, 1037–1039. https://doi.org/10.1080/15548627.2021.1883886.

44. Trajkovic, K., Jeong, H., and Krainc, D. (2017). Mutant huntingtin is secreted via a late endosomal/lysosomal unconventional secretory pathway. J. Neurosci. *37*, 9000–9012. https://doi.org/10.1523/JNEUROSCI.0118-17.2017.

45. Bobrie, A., Colombo, M., Krumeich, S., Raposo, G., and Théry, C. (2012). Diverse subpopulations of vesicles secreted by different intracellular mechanisms are present in exosome preparations obtained by differential ultracentrifugation. J. Extracell. Vesicles *1*, 18397. https://doi.org/10.3402/jev.v1i0.18397.

46. Gentile, F., Calì, G., Zurzolo, C., Corteggio, A., Rosa, P., Calegari, F., Levi, A., Possenti, R., Puri, C., Tacchetti, C., and Nitsch, L. (2004). The neuroendocrine protein VGF is sorted into dense-core granules and is secreted apically by polarized rat thyroid epithelial cells. Exp. Cell Res. *295*, 269–280. https://doi.org/10.1016/j.yexcr.2004.01.010.

47. Verderio, C., Cagnoli, C., Bergami, M., Francolini, M., Schenk, U., Colombo, A., Riganti, L., Frassoni, C., Zuccaro, E., Danglot, L., et al. (2012). TI-VAMP/VAMP7 is the SNARE of secretory lysosomes contributing to ATP secretion from astrocytes. Biol. Cell *104*, 213–228. https://doi.org/10.1111/boc.201100070.

48. Bonifacino, J.S., and Neefjes, J. (2017). Moving and positioning the endolysosomal system. Curr. Opin. Cell Biol. *47*, 1–8. https://doi.org/10.1016/j.ceb.2017.01.008.

49. Molino, D., Nola, S., Lam, S.M., Verraes, A., Proux-Gillardeaux, V., Boncompain, G., Perez, F., Wenk, M., Shui, G., Danglot, L., and Galli, T. (2015). Role of tetanus neurotoxin insensitive vesicle-associated membrane protein in membrane domains transport and homeostasis. Cell. Logist. *5*, e1025182. https://doi.org/10.1080/21592799.2015.1025182.

50. Sikora, R., Bun, P., Danglot, L., Alqabandi, M., Bassereau, P., Niedergang, F., Galli, T., and Zahraoui, A. (2021). MICAL-L1 is required for cargo protein delivery to the cell surface. Biol. Open *10*, bio058008. https://doi.org/10.1242/bio.058008.

51. Eidson, L.N., Kannarkat, G.T., Barnum, C.J., Chang, J., Chung, J., Caspell-Garcia, C., Taylor, P., Mollenhauer, B., Schlossmacher, M.G., Ereshefsky, L., et al. (2017). Candidate inflammatory biomarkers display unique relationships with alpha-synuclein and correlate with measures of disease severity in subjects with Parkinson's disease. J. Neuroinflammation *14*, 164. https://doi.org/10.1186/s12974-017-0935-1.

52. Fourriere, L., Divoux, S., Roceri, M., Perez, F., and Boncompain, G. (2016). Microtubule-independent secretion requires functional maturation of Golgi elements. J. Cell Sci. *129*, 3238–3250. https://doi.org/10.1242/jcs.188870.

53. Proux-Gillardeaux, V., Raposo, G., Irinopoulou, T., and Galli, T. (2007). Expression of the Longin domain of TI-VAMP impairs lysosomal secretion and epithelial cell migration. Biol. Cell *99*, 261–271. https://doi.org/10.1042/BC20060097.

54. Gupton, S.L., and Gertler, F.B. (2010). Integrin signaling switches the cytoskeletal and exocytic machinery that drives neuritogenesis. Dev. Cell *18*, 725–736. https://doi.org/10.1016/j.devcel.2010.02.017.

55. Xie, Y.X., Naseri, N.N., Fels, J., Kharel, P., Na, Y., Lane, D., Burré, J., and Sharma, M. (2022). Lysosomal exocytosis releases pathogenic α-synuclein species from neurons in synucleinopathy models. Nat. Commun. *13*, 4918. https://doi.org/10.1038/s41467-022-32625-1.

56. Rivero-Ríos, P., Romo-Lozano, M., Madero-Pérez, J., Thomas, A.P., Biosa, A., Greggio, E., and Hilfiker, S. (2019). The G2019S variant of leucine-rich repeat kinase 2 (LRRK2) alters endolysosomal trafficking by impairing the function of the GTPase RAB8A. J. Biol. Chem. *294*, 4738–4758. https://doi.org/10.1074/jbc.RA118.005008.

57. Cookson, M.R. (2016). Cellular functions of LRRK2 implicate vesicular trafficking pathways in Parkinson's disease. Biochem. Soc. Trans. *44*, 1603–1610. https://doi.org/10.1042/BST20160228.

58. Kedashiro, S., Pastuhov, S.I., Nishioka, T., Watanabe, T., Kaibuchi, K., Matsumoto, K., and Hanafusa, H. (2015). LRRK1-phosphorylated CLIP-170 regulates EGFR trafficking by recruiting p150Glued to microtubule plus ends. J. Cell Sci. *128*, 829. https://doi.org/10.1242/jcs.169102.

59. Lin, C.-H., Li, H., Lee, Y.-N., Cheng, Y.-J., Wu, R.-M., and Chien, C.-T. (2015). Lrrk regulates the dynamic profile of dendritic Golgi outposts through the golgin Lava lamp. J. Cell Biol. *210*, 471–483. https://doi.org/10.1083/jcb.201411033.

60. Boecker, C.A., Goldsmith, J., Dou, D., Cajka, G.G., and Holzbaur, E.L.F. (2021). Increased LRRK2 kinase activity alters neuronal autophagy by disrupting the axonal transport of autophagosomes. Curr. Biol. *31*, 2140–2154.e6. https://doi.org/10.1016/j.cub.2021.02.061.

61. Brzozowski, C.F., Hijaz, B.A., Singh, V., Gcwensa, N.Z., Kelly, K., Boyden, E.S., West, A.B., Sarkar, D., and Volpicelli-Daley, L.A. (2021). Inhibition of LRRK2 kinase activity promotes anterograde axonal transport and presynaptic targeting of α-synuclein. Acta Neuropathol. Commun. *9*, 180. https://doi.org/10.1186/s40478-021-01283-7.

62. Deniston, C.K., Salogiannis, J., Mathea, S., Snead, D.M., Lahiri, I., Matyszewski, M., Donosa, O., Watanabe, R., Böhning, J., Shiau, A.K., et al. (2020). Structure of LRRK2 in Parkinson's disease and model for microtubule interaction. Nature *588*, 344–349. https://doi.org/10.1038/s41586-020-2673-2.

63. Chilcote, T.J., Galli, T., Mundigl, O., Edelmann, L., McPherson, P.S., Takei, K., and De Camilli, P. (1995). Cellubrevin and synaptobrevins: similar subcellular localization and biochemical properties in PC12 cells. J. Cell Biol. *129*, 219–231. https://doi.org/10.1083/jcb.129.1.219.

64. Moore, H.P.H., Andresen, J.M., Eaton, B.A., Grabe, M., Haugwitz, M., Wu, M.M., and Machen, T.E. (2002). Biosynthesis and secretion of pituitary hormones: dynamics and regulation. Arch. Physiol. Biochem. *110*, 16–25. https://doi.org/10.1076/apab.110.1.16.903.

65. Li, M., Feng, F., Feng, H., Hu, P., Xue, Y., Xu, T., and Song, E. (2022). VAMP4 regulates insulin levels by targeting secretory granules to lysosomes. J. Cell Biol. *221*, e202110164. https://doi.org/10.1083/jcb.202110164.

66. Vats, S., and Galli, T. (2022). Role of SNAREs in unconventional secretion-focus on the VAMP7-dependent secretion. Front. Cell Dev. Biol. *10*, 884020. https://doi.org/10.3389/fcell.2022.884020.

67. Reddy, A., Caler, E.V., and Andrews, N.W. (2001). Plasma membrane repair is mediated by Ca(2+)-regulated exocytosis of lysosomes. Cell *106*, 157–169. https://doi.org/10.1016/s0092-8674(01)00421-4.

68. Fader, C.M., Aguilera, M.O., and Colombo, M.I. (2012). ATP is released from autophagic vesicles to the extracellular space in a VAMP7-dependent manner. Autophagy *8*, 1741–1756. https://doi.org/10.4161/auto.21858.

69. Johnson, D.E., Ostrowski, P., Jaumouillé, V., and Grinstein, S. (2016). The position of lysosomes within the cell determines their luminal pH. J. Cell Biol. *212*, 677–692. https://doi.org/10.1083/jcb.201507112.

70. Barral, D.C., Staiano, L., Guimas Almeida, C., Cutler, D.F., Eden, E.R., Futter, C.E., Galione, A., Marques, A.R.A., Medina, D.L., Napolitano, G., et al. (2022). Current methods to analyze lysosome morphology, positioning, motility and function. Traffic *23*, 238–269. https://doi.org/10.1111/tra.12839.

71. Ghosh, D., Pinto, S., Danglot, L., Vandewauw, I., Segal, A., Van Ranst, N., Benoit, M., Janssens, A., Vennekens, R., Vanden Berghe, P., et al. (2016). VAMP7 regulates constitutive membrane incorporation of the cold-activated channel TRPM8. Nat. Commun. *7*, 10489. https://doi.org/10.1038/ncomms10489.

72. Parashar, S., Chidambaram, R., Chen, S., Liem, C.R., Griffis, E., Lambert, G.G., Shaner, N.C., Wortham, M., Hay, J.C., and Ferro-Novick, S. (2021). Endoplasmic reticulum tubules limit the size of misfolded protein condensates. Elife *10*, e71642. https://doi.org/10.7554/eLife.71642.

73. Laguerre, F., Anouar, Y., and Montero-Hadjadje, M. (2020). Chromogranin A in the early steps of the neurosecretory pathway. IUBMB Life *72*, 524–532. https://doi.org/10.1002/iub.2218.

74. Panicker, N., Ge, P., Dawson, V.L., and Dawson, T.M. (2021). The cell biology of Parkinson's disease. J. Cell Biol. *220*, e202012095. https://doi.org/10.1083/jcb.202012095.

75. Kandachar, V., Tam, B.M., Moritz, O.L., and Deretic, D. (2018). An interaction network between the SNARE VAMP7 and Rab GTPases within a ciliary membrane-targeting complex. J. Cell Sci. *131*, jcs222034. https://doi.org/10.1242/jcs.222034.

76. Kaech, S., and Banker, G. (2006). Culturing hippocampal neurons. Nat. Protoc. *1*, 2406–2415. https://doi.org/10.1038/nprot.2006.356.

77. Ran, F.A., Hsu, P.D., Wright, J., Agarwala, V., Scott, D.A., and Zhang, F. (2013). Genome engineering using the CRISPR-Cas9 system. Nat. Protoc. *8*, 2281–2308. https://doi.org/10.1038/nprot.2013.143.

78. Chari, R., Yeo, N.C., Chavez, A., and Church, G.M. (2017). sgRNA scorer 2.0: a species-independent model to predict CRISPR/cas9 activity. ACS Synth. Biol. *6*, 902–904. https://doi.org/10.1021/acssynbio.6b00343.

79. Gibson, D.G., Glass, J.I., Lartigue, C., Noskov, V.N., Chuang, R.-Y., Algire, M.A., Benders, G.A., Montague, M.G., Ma, L., Moodie, M.M., et al. (2010). Creation of a bacterial cell controlled by a chemically synthesized genome. Science *329*, 52–56. https://doi.org/10.1126/science.1190719.

80. Cox, J., and Mann, M. (2008). MaxQuant enables high peptide identification rates, individualized p.p.b.-range mass accuracies and proteome-wide protein quantification. Nat. Biotechnol. *26*, 1367–1372. https://doi.org/10.1038/nbt.1511.

81. Tyanova, S., Temu, T., Sinitcyn, P., Carlson, A., Hein, M.Y., Geiger, T., Mann, M., and Cox, J. (2016). The Perseus computational platform for comprehensive analysis of (prote)omics data. Nat. Methods *13*, 731–740. https://doi.org/10.1038/nmeth.3901.

82. Kuleshov, M.V., Jones, M.R., Rouillard, A.D., Fernandez, N.F., Duan, Q., Wang, Z., Koplev, S., Jenkins, S.L., Jagodnik, K.M., Lachmann, A., et al. (2016). Enrichr: a comprehensive gene set enrichment analysis web server 2016 update. Nucleic Acids Res. *44*, W90–W97. https://doi.org/10.1093/nar/gkw377.

83. Vojtek, A.B., and Hollenberg, S.M. (1995). Ras-Raf interaction: two-hybrid analysis. Methods Enzymol. *255*, 331–342.

84. Béranger, F., Aresta, S., de Gunzburg, J., and Camonis, J. (1997). Getting more from the two-hybrid system: N-terminal fusions to LexA are efficient and sensitive baits for two-hybrid studies. Nucleic Acids Res. *25*, 2035–2036. https://doi.org/10.1093/nar/25.10.2035.

85. Bartel, P., Chien, C.T., Sternglanz, R., and Fields, S. (1993). Elimination of false positives that arise in using the two-hybrid system. Biotechniques *14*, 920–924.

86. Fromont-Racine, M., Rain, J.-C., and Legrain, P. (2002). Building protein-protein networks by two-hybrid mating strategy. In Guide to Yeast Genetics and Molecular and Cell Biology - Part B Methods in Enzymology (Elsevier), pp. 513–524. https://doi.org/10.1016/S0076-6879(02)50982-4.

87. Schindelin, J., Arganda-Carreras, I., Frise, E., Kaynig, V., Longair, M., Pietzsch, T., Preibisch, S., Rueden, C., Saalfeld, S., Schmid, B., et al. (2012). Fiji: an open-source platform for biological-image analysis. Nat. Methods *9*, 676–682. https://doi.org/10.1038/nmeth.2019.

88. de Chaumont, F., Dallongeville, S., Chenouard, N., Hervé, N., Pop, S., Provoost, T., Meas-Yedid, V., Pankajakshan, P., Lecomte, T., Le Montagner, Y., et al. (2012). Icy: an open bioimage informatics platform for extended reproducible research. Nat. Methods *9*, 690–696. https://doi.org/10.1038/nmeth.2075.

89. Lord, S.J., Velle, K.B., Mullins, R.D., and Fritz-Laylin, L.K. (2020). SuperPlots: communicating reproducibility and variability in cell biology. J. Cell Biol. *219*, e202001064. https://doi.org/10.1083/jcb.202001064.

STAR★METHODS

KEY RESOURCES TABLE

REAGENT or RESOURCE	SOURCE	IDENTIFIER
Antibodies		
Anti CD63	BD Biosciences	Cat# 551458; RRID:AB_394205
Anti GAPDH	Sigma-Aldrich	Cat# G9545; RRID:AB_796208
Anti GFP serum	N/A	rpAb TG32
Anti GFP purified	Roche	Roche Cat# 11814460001; RRID:AB_390913
Anti GM130	BD Biosciences	Cat# 610823; RRID:AB_398142
Anti HSC70	Santa Cruz Biotechnologies	Cat# sc-1059; RRID:AB_2120291
Anti LAMP1	Sigma-Aldrich	Cat# L1418; RRID:AB_477157
Anti LRRK2 purified	Abcam	Cat # ab133474; RRID:AB_2713963
Anti LRRK2 serum	Antibodies Incorporated	Cat# 73–253; RRID:AB_10671178
Anti TGN46	Bio-rad	Cat# AHP500GT; RRID:AB_2203291
Anti TSG101	Genetex	Cat# GTX70255; RRID:AB_373239
Anti VAMP2	N/A	mAB 69.1
Anti VAMP4	N/A	rpAb TG19B
Anti VAMP7	N/A	rpAb TG50
Anti VGF	Santa Cruz Biotechnology	Cat# sc-365397; RRID:AB_10846955
Deposited data		
Analyzed Proteomic Dataset from PC12 cells	This manuscript	ProteomeXchange Consortium via PRIDE, ID = PXD028321 https://www.ebi.ac.uk/pride/archive/projects/PXD028321
Proteomics results with legends are summarized in Table S1	This manuscript	N/A
Experimental models: Cell lines		
PC12	ATCC	Cat# CRL-1721.1
HEK293T	Evelyne Bloch-Gallego, Institut Cochin	N/A
Oligonucleotides		
Guide RNA to KO VAMP 2 CACCgTGGCAGCGGTAGCCGACCTAAAAC TAGGTCGGCTACCGCTGCCAc	This manuscript	N/A
Guide RNA to KO VAMP 4 CACCgTTTAGGTGGCGCTTGAACTTAAACA AGTTCAAGCGCCACCTAAAc	This manuscript	N/A
See Table S2 for primers used for cloning	This manuscript	N/A
Recombinant DNA		
See Table S2 for cloning details (initial plasmids, primers, cloning methods used)	This manuscript	N/A
RFP-VAMP4	This manuscript	N/A
mCherry-LRRK2 WT	This manuscript	N/A
mCherry-LRRK2 G2019S	This manuscript	N/A
mCherry-LRRK2 R1441C	This manuscript	N/A
RUSH-VGF-mCherry	This manuscript	N/A

(*Continued on next page*)

Continued

REAGENT or RESOURCE	SOURCE	IDENTIFIER
pDEST53-LRRK2-WT	Mark Cookson	RRID: Addgene_25044
pDEST53-LRRK2-G2019S	Mark Cookson	RRID:Addgene_25045
pDEST53-LRRK2-R1441C	Mark Cookson	RRID:Addgene_25046
CMV-VGF	Andrea Levi	RRID:Addgene_107575
pSpCas9(BB)-2A-GFP (PX458)	Feng Zhang	RRID:Addgene_48138
Str-KDEL_TNF-SBP-mCherry	Franck Perez	RRID:Addgene_65279
pEGFP-Snapin	Beverly Koller	RRID:Addgene_118742
p3Flag-CMV10-LRRK2-WT	Marie-Christine Chartier-Harlin and Jean-Marc Taymans	N/A
pGEX-GST-VAMP4$^{(1-117)}$	(Mallard et al.)[26]	N/A
pGEX-GST-VAMP7$^{(1-184)}$	(Martinez-Arca et al.)[30]	N/A
N-acetyl Glucosamine Transferase-GFP (NAGT-GFP)	Kohji Takei	N/A
Software and algorithms		
ImageJ/Fiji	https://imagej.net/software/fiji/	N/A
Icy	http://icy.bioimageanalysis.org/	N/A
Prism v5.03 GraphPad software	https://www.graphpad.com/scientific-software/prism/	N/A

RESOURCE AVAILABILITY

Lead contact

Further information and requests for resources and reagents should be directed to and will be fulfilled by the Lead Contact, Thierry Galli (thierry.galli@inserm.fr).

Materials availability

Plasmids and cell lines generated in this study have not been deposited to any public repository and are available upon reasonable request to the lead contact.

Data and code availability

- The mass spectrometry proteomic data have been deposited at the ProteomeXchange Consortium via the PRIDE partner repository with the dataset identifier PXD028321 (https://www.ebi.ac.uk/pride/archive/projects/PXD028321).
- This paper does not report original code.
- Other data are available upon reasonable request to the lead contact.

EXPERIMENTAL MODELS AND SUBJECT DETAILS

Cell lines

Human Embryonic Kidney (HEK293T) cells were obtained from Evelyne Bloch-Gallego, Institut Cochin, Paris, France and cultured in DMEM medium (Fisher Scientific 41966052) supplemented by 10% of Fetal Bovine Serum (Biosera FB – 1001/500), 5% of glutamine (Thermofisher 35050038) and 2,5% of penicillin streptomycin (Life Technologies 15140122) and maintained at 37°C with 5% of CO_2.

PC12 cells (ATCC Cat# CRL-1721.1) were cultured in RPMI 1640 medium (Life Technologies 21875034) supplemented with 10% Horse Serum (Biosera DH-291H/500), 5% of Fetal Bovine Serum (Biosera FB – 1001/500) and 1% of Penicillin-Streptomycin (Life Technologies 15140122) and maintained at 37°C with 5% of CO_2. Petri culture dishes were coated to help cell adhesion by using a 1 mg/mL collagen (Sigma C7661) solution diluted to obtain 1.83 $\mu g/cm^2$ on the plastic. For NGF-experiments, cells were cultured in low-concentration of serum RPMI 1640 (1% of Horse Serum) for one week and supplemented with 50 ng/mL NGF (Sigma-Aldrich N1408-1MG) to induce neurite-like extensions.

Primary culture

Following ethical guidelines (CEEA - 034 Comité d'éthique en matière d'expérimentation animale Paris Descartes), in agreement with Directive 2010/63/EU as amended by Regulation (EU) 2019/1010, pregnant rats were terminally anesthetized with CO_2 before removing the embryos which were decapitated immediately. Primary neuronal cultures were prepared as previously described.[76]

E18-E19 rat hippocampal neurons were dissected, enzymatically dissociated and plated onto poly-D-lysine coated glass coverslips (1 mg/mL) in Neurobasal (Thermofisher 21103049) with 1X B-27 (Thermofisher 17504044) and Glutamax (Thermofisher 35050038). After 2 to 4 h, the culture media was changed with conditioned neuronal B-27 media. Hippocampal neurons were plated on 18 mm pre-coated coverslips at a density of 13,000 neurons/cm2, transfected with Lipofectamine 2000 (Thermofisher 11668027) at DIV6 and fixed at DIV8.

METHOD DETAILS

CRISPR/Cas9 genetic engineering

In order to generate the knockout PC12 cell lines present in our study, we used the RNA-guided Cas9 endonuclease from the microbial clustered regularly interspaced short palindromic repeats (CRISPR) adaptive immune system.[77] The guide RNAs were designed and chosen by using the selection tool CRISPOR which outputs scores based on potential off-target and on-target DNA cleavage activity.[78] The 2 highest-scored guide RNAs sequences were cloned into a pSpCas9(BB)-2A-GFP backbone plasmid. The correct insertion was confirmed by colony PCR and sequencing. Plasmids were further amplified, purified and electroporated to PC12 cells with a Bio-Rad electroporation device which allowed high number of positive cells with moderate plasmid expression. The following day, cells were trypsinized and detached from the culture dish, pelleted and resuspended in PBS $CaCl_2$/$MgCl_2$ free, EDTA 1 mM, 25 mM HEPES, 1% fetal bovine serum, penicillin and streptomycin. Cells were then sorted by a Fluorescence Activated Cell Sorter by placing one GFP-positive cell per well in a 96-multi well plate containing complete media supplemented with penicillin, streptomycin and kanamycin. Confirmation of gene knockout was conducted by performing protein electrophoresis and Western Blot.

Plasmids

Plasmids used in this study are listed in the key resources table.

Cloning was performed using Gibson assembly reaction.[79] PCR were conducted using Q5 polymerase (New England Biolabs, #M0491S) using provider's guidelines and handmade Gibson assembly mix (Miller's lab). See Table S2 for list of plasmids and primers used for cloning.

Protein electrophoresis and Western blot

Cells were briefly washed with D-PBS ($CaCl_2$/$MgCl_2$) and proteins were extracted by using a lysis buffer (TSE) composed of Tris 50 mM; NaCl 150 mM; EDTA 10 mM supplemented with Triton X-100 1% and 1X protease inhibitor cocktail (Sigma 05056489001). After 20 min at 4°C, cells were centrifuged at 16,000 x *g* for 30 min at 4°C and supernatants were recovered. Proteins (15–30 μg) were diluted in beta-mercaptoethanol sample buffer, loaded into 4–12% Tris-Glycine or Bis-Tris gradient gels (Life Technologies XP04125BOX; NP0336BOX) and run at 100–130 V for 90 min. Proteins were transferred into 0.45 μm nitrocellulose membranes at 100V/500 mA for 90 min at 4°C. Membranes were then blocked with 5% of non-fat dry milk diluted in a Tris-based saline solution with 0.1% of Tween 20 (TBST). Primary antibodies were incubated with the same solution overnight at 4°C. After 3 washes with TBST solution, HRP-coupled secondary antibodies were incubated for 45 min in TBST. After washes in TBST, membranes were incubated with SuperSignal West Femto Maximum Sensitivity Substrate (Thermo Fisher 34095) and signal was detected with a Chemidoc imager (Bio-Rad).

Immunoprecipitation

Co-immunoprecipitation experiments were performed by seeding HEK293T cells into 60 mm plastic culture dishes (TPP 1613483). Cell density was established with Luna automated cell counter (LogosBio L10001). Co-transfection was performed using JetPrime (Ozyme POL114-15) according to manufacturer's protocol with the required constructs. Proteins were extracted from cells with TSE as described above 48h after transfection. Dynabeads Protein A (Life Technologies 10001D) were coupled with the homemade GFP antibody TG32 for 20 min. Cell extracts (1 mg) for each condition was then incubated with coupled beads for 1h at 4°C and then washed 5 times with lysis buffer to avoid unspecific bindings.

For sequential immunoprecipitation experiment, cell extracts were obtained as previously described except they were initially cross-linked with 25 mM DSP (Thermo Fisher 22585) following manufacturer's protocol. GFP-Snapin associated complexes were isolated by incubating (90 min, 4°C) cell lysates (1.5 mg per condition) with 0.4 nmol GFP-Binding-Protein-Strep-tag (GBP-st) pre-coupled to Strep-Tactin Sepharose beads (IBA 21201010). Part of the complexes was eluted using 12.5 mM desthiobiotin (IBA 2-1000-001) for 15 min and submitted to second immunoprecipitation as previously described, using rabbit anti-LRRK2 antibody coupled to Dynabeads M-280 Sheep Anti-Rabbit IgG (Life Technologies 11203D; "IP #2"). Non-eluted complexes were recovered from GBP-st beads by incubating with 2X sample buffer at 95°C for 10 min ("IP #1").

All immunoprecipitated fractions were resuspended in sample buffer and boiled prior SDS-PAGE then immunoblotted as described above.

GST pull-down

LRRK2 protein was produced and purified as already described.[36] GST-tagged cytosolic form of VAMP4 and VAMP7, and GST only were generated by the Biochemistry and Biophysics (B&B) facility of the Institute of Psychiatry and Neuroscience of Paris (IPNP).

Briefly, BL21 bacteria were transformed with corresponding plasmid. Production was performed in LB and induced with IPTG 1 mM for 3h at 37°C. Pelleted bacteria were lysed (25 mM HEPES/KOH pH 7.5, 400 mM KCl, 10% Glycerol, 1 mM DTT, 4% Triton X-100, 10 mM $MgCl_2$, Protease Inhibitor Cocktail, DNAse) and sonicated. After centrifugation, purification was performed on AKTA Pure 25M (Cytiva) with GSTrap HP column (Cytiva 17528201). Column was washed in PBS and bound proteins were eluted 10 mM reduced L-Gluthatione (Sigma-Aldrich G4251) in 50 mM Tris-HCl pH 8.

For pull-down experiments, anti-GST magnetic beads (Sigma G0924) were washed in TSE and pre-loaded with GST-tagged proteins by incubation 1h on wheel at 4°C. After washing of coupled beads with TSE and addition of BSA (1 μM final), the equivalent of 300 pmol of GST-tagged protein and 30 pmol of LRRK2 were incubated 1h on wheel at 4°C. After extensive washes, beads were resuspended in sample buffer and boiled prior SDS-PAGE.

Secretion assay

PC12 cells of different genotypes were seeded into 60 mm culture dishes (TPP 1613483) and NGF-differentiated for one week as described above. On day 6, cells were gently washed in PBS and incubated 16h with RPMI 1640 without serum in order to avoid albumin and other seric proteins contamination. Harvested culture media were collected and centrifuged at 2,000 x *g* for 20 min at 4°C, to remove cell debris.

The recovered supernatants were submitted to (i) acetone precipitation and/or (ii) sequential centrifugation. (i) Four volumes of acetone were added to supernatants, thoroughly mixed and incubated overnight at −20°C. After 16,000 x *g*/30 min centrifugation, supernatants were discarded and concentrated total secreted proteins were recovered by resuspending the pellet in TSE (“Total release”). (ii) For sequential centrifugation, debris-free supernatants were transferred to ultracentrifugation tubes (Beckman 344057) and first spun down in SW55Ti rotor using OPTIMA XPN-80 Ultra ultracentrifuge (Beckman) at 15,000 x *g* for 30 min at 4°C. Supernatants were carefully transferred to new ultracentrifugation tubes while pellets were gently washed in PBS and resuspended in TSE buffer (“15K pellet”). Recovered supernatants were then centrifuged at 200,000 x *g* for 60 min at 4°C and pellets were resuspended in TSE buffer (“200K pellet”). Cell lysates (“Cell content”) and 1/3 of the corresponding secreted fraction were loaded into 4–12% Bis-Tris gradient gels (Life Technologies NP0336BOX), transferred and immunoblotted as abovementioned.

Extracellular vesicles size distribution and concentration were assessed by multi-angle dynamic light scattering and performed at the B&B facility of the IPNP using the Zetasizer Ultra-Red apparatus (Malvern Instruments). The different fractions (15K/200K) were obtained as abovementioned except pellets were resuspended in RPMI 1640. The multiangle tank (Cell ZEN2112) was pre-cleaned twice with pure water and ethanol 20%, once with pure ethanol and twice with RPMI 1640 between each measurement. The software was set up with the following parameters: Material protein, Dispersant water, Back Scatter Manual = 11, Measurements Manual = 20. “RPMI 1640 only” condition was used as blank.

Immunofluorescence

For immunostaining, cells were briefly washed with D-PBS ($CaCl_2$/$MgCl_2$) and then fixed in 4% paraformaldehyde (Sigma 441244-1KG) for 20 min at room temperature, followed by quenching of the reaction with 40 mM PBS NH_4Cl. Cells were permeabilized with 0.1% Triton X-100 for 5 min followed by 3 washes in PBS. To saturate unspecific bindings of the antibodies, cells were then blocked with a solution made of 10% serum from the species the secondary antibody was raised in. Incubation of primary antibodies was made in a solution of 1/3 serum, Triton X-100 0.1% diluted in PBS for 1h at room temperature or overnight at 4°C in a humidified chamber. Cells were then washed 3 times in PBS and incubated for 45 min at room temperature with secondary antibodies conjugated with fluorescent probes Alexa 488, 568 of 647 together with DAPI (Life Technologies). After 3 washes in PBS, coverslips were mounted with Prolong Gold (Life Technologies P36930) mounting media.

RUSH assay

RUSH plasmids were used as previously described.[34] Principle of the RUSH assay is depicted in Figure 5A. Briefly, we transfected HEK293T cells with RUSH plasmids encoding an ER hook and mCherry as reporter. Cells were cultured in DMEM + FBS lacking biotin (from Franck Perez’ lab). Upon addition of biotin at 40 μM, cells were either live imaged or fixed at indicated timepoints before immunostaining.

Live cell imaging

HEK293T were seeded on poly-D-ornithine (1 mg/ml) pre-coated glass coverslips and transfected with RUSH-VGF-mCherry plasmid and NAGT-GFP plasmids (ratio 1:1) using JetPrime (Ozyme POL114-15) in biotin-free culture media as mentioned before. The following day, coverslips were transferred to Chamlide EC-B18 imaging chamber and maintained in Krebs-Ringer buffer (140 mM NaCl, 2.5 mM KCl, 1.8 mM $CaCl_2$, 1 mM $MgCl_2$, 20 mM HEPES, 4.5 g/ml glucose and pH 7.4). The chamber was placed in a Leica DMI6000B inverted microscope with a Leica 63X/1.4 NA Plan-Apochromat oil immersion objective plus a 1.6× mag changer and an ImagEMX2 EMCCD camera (Hamamatsu). Diode-pumped 25 mW, 561 nm (Melles Griot) and 200 mW, 488 nm (Nichia) lasers were used as light sources and were controlled by iLas2 targeted-laser illumination controller (Roper). The microscopy system was managed by Metamorph software (Molecular Devices). Multi-position and Z-stack acquisition started when biotin (40μM final) was added to the media, lasted 90 min with a rate of one new acquisition every 30 s.

Confocal imaging

Z-stack confocal imaging was carried out on a TCS SP5 (63X, NA 1.4, oil immersion objective) microscope equipped with a resonant scanner (8 kHz). Detection was made with 3 PMTs (photomultiplier modules), or with a highly sensitive hybrid detector. Images were acquired with given laser and spectral bands allowing to avoid signal bleed-through.

Proteomic analysis

The secretome samples were prepared as mentioned above and first precipitated with 10% TCA (trichloroacetic acid) at −20°C, overnight, centrifuged at 20,000 x *g* and washed 4 times with 100% ethanol. The final pellets were resuspended in 50μL of 5% SDS in 100mM TEAB buffer, supplemented with 20mM TCEP and 50mM CAA (chloracetamide) and incubated for 5 min at 95°C. S-Trap micro spin column (Protifi, Hutington, USA) digestion was performed on 50μg of total lysate samples and on secretome samples, according to manufacturer's instructions. Briefly, lysate samples were first reduced with 20mM TCEP and alkylated with 50mM CAA for 15 min at room temperature. Aqueous phosphoric acid was then added to all samples to a final concentration of 1.2% following by the addition of S-Trap binding buffer (90% aqueous methanol, 100mM TEAB, pH 7.1). Mixtures were then loaded on S-Trap columns. Two extra washing steps were performed for thorough SDS elimination. Samples were digested with 2.5μg of trypsin (Promega) at 47°C for 1 h. After elution, peptides were vacuum dried.

The tryptic peptides were resuspended in 100μL of 2% acetonitrile, 0.1% formic acid and 1μL was injected on a nanoElute (Bruker Daltonics, Germany) HPLC (high-performance liquid chromatography) system coupled to a timsTOF Pro (Bruker Daltonics, Germany) mass spectrometer. HPLC separation (Solvent A: 0.1% formic acid in water, 2% acetonitrile; Solvent B: 0.1% formic acid in acetonitrile) was carried out at 300 nL/min using a packed emitter column (C18, 25 cm × 75μm 1.6μm) (Ion Optics, Australia) using a gradient elution (2–10% solvent B during 40 min; 10 to 15% during 23 min; 15%–25% during 27 min; 25%–80% for 10 min and finally 80% for 5 min to wash the column). Mass-spectrometric data were acquired using the parallel accumulation serial fragmentation (PASEF) acquisition method. The measurements were carried out over the m/z range from 100 to 1700 Th. The range of ion mobilities values from 0.8 to 1.3 V s/cm^2 (1/k0). The total cycle time was set to 1.17s and the number of PASEF MS/MS scans was set to 10.

The MS files were processed with the MaxQuant[80] software version 1.6.17.0 and searched with Andromeda search engine against the UniProtKB/Swiss-Prot *Rattus norvegicus* database mixed with its trEMBL entries (updated February 2021, 36188 entries). To search parent mass and fragment ions, we set a mass deviation of 10 ppm and 40 ppm respectively. The minimum peptide length was set to 7 amino acids and strict specificity for Trypsin/P cleavage was required, allowing up to two missed cleavage sites. Carbamidomethylation (Cys) was set as fixed modification, whereas oxidation (Met) and N-term protein acetylation were set as variable modifications. The false discovery rates (FDRs) at the protein and peptide level were set to 1%. Scores were calculated in MaxQuant as described previously.[80] The reverse and common contaminants hits were removed from MaxQuant output. Proteins were quantified according to the MaxQuant label-free algorithm using LFQ intensities; protein quantification was obtained using at least 2 peptides per protein and match between runs was allowed across samples.

Statistical and bioinformatic analysis, including heatmaps, profile plots and clustering, were performed with Perseus software (version 1.6.14.0) freely available at www.perseus-framework.org.[81] For statistical comparison, we set 3 groups, each containing up to 3 biological replicates. We then filtered the data to keep only proteins with at least 3 valid values in at least one group. Next, the data were imputed to fill missing data points by creating a Gaussian distribution of random numbers with a standard deviation of 30% relative to the standard deviation of the measured values and 1.8 standard deviation downshift of the mean to simulate the distribution of low signal values. We performed an ANOVA test, FDR<0.05, S0 = 0.1 on both cell lysate and secretome sample groups and Student t-test, FDR<0.05, S0 = 0.1 or S0 = 1 for cell lysate and secretome sample groups, respectively.

Finally, the differentially expressed proteins were subjected to bioinformatic analysis using EnrichR software freely available at http://maayanlab.cloud/Enrichr/for enrichment of GO terms using GO Cellular Component library from 2018.[82] Ranking of enriched term was performed using combined score which is a combination of the p value and *Z* score calculated by multiplying both scores as follows: c = ln(p) *z (see Help page of website for more details) where high value of combined score shows highly significant GO term.

Yeast two-hybrid (Y2H)

The LRRK2 library screening and direct 1-by-1 interaction assay were performed by Hybrigenics Services SAS, Paris, France (http://www.hybrigenics-services.com) as described below.

Cloning

The coding sequence of the human VAMP7 wt (aa 1–188, GenBank accession number NM_005638.3), the human VAMP4 (aa 1–117, GenBank accession number NM_003762.1), was PCR-amplified and cloned in frame with the LexA DNA binding domain (DBD) into plasmid pB29 as an N-terminal fusion to LexA (bait-LexA fusion). The human Snapin (aa 1–136, GenBank accession number NM_012437.5) was PCR-amplified and cloned in frame with the LexA DNA binding domain (DBD) into pB27 as a C-terminal fusion to LexA (LexA-bait fusion). pB27 and pB29 derive from the original pBTM116 vector.[83,84] Hybrigenics' references for those constructs are hgx425v2_pB29, hgx3438v1_pB29, hgx710v1_pB29, hgx1310v2_pB27 respectively.

LRRK2 cDNA (NM_198578.3) was subcloned in LexA bait vector pB27 derive from pLexA[83] using oligonucleotide 6690 (CAGGGCAATAAAGTCGAACT) and 6972 (GACCTACAGGAAAGAGTTACTC). 5 μg of the PCR product was subjected to Fragmentase treatment (New England Biolab, NEB) until a smear of fragments was detected around 500pb by agarose gel electrophoresis. The DNA fragments were purified by phenol/chloroform extraction and ethanol precipitation. The DNA fragments were next

subjected to end repair (NEB) and dA-tailing adaptation, using Blunt/TA ligase master mix with NEBNext Adaptor hairpin loop (NEB), followed by AMPure XP bead (Beckman Coulter) purification. After USER enzyme digestion (NEB), DNA fragments were amplified with oligonucleotides 10,829 (CTATTCGATGATGAAGATACCCCACCAAACCCAAAAAAAGAGATCCTAGAACTAGACACTCTTTCCCTACACGACGCTCTTCCGATCT) and 10,830 (CCGGGCCTCTAGACACTAGCTACTCGAGGGGCCCCAGTGGCCCTATCTATGCGGCCGCTCAGACTGGAGTTCAGACGTGTGCTCTTCCGATC) with 15 cycles of PCR using NEBNext Q5 Hot Start HiFi PCR Master Mix (NEB), which allowed to add Gap Repair recombination sequences for the cloning in Gal4-AD prey plasmid pP9 derived from the original pGADGH.[85] The library comprised 44,500 independent clones.

The fragment corresponding to amino acids 1773–1857 of human LRRK2 was extracted from the ULTImate Y2H screening of Snapin with a library of fragments of LRRK2. It is cloned in frame with the Gal4 activation domain (AD) into plasmid pP6, derived from the original pGADGH.[85] The AD construct was checked by sequencing.

1-By-1 Y2H interaction assays

Bait and prey constructs were transformed in the yeast haploid cells L40ΔGal4 (mata) and YHGX13 (Y187 ade2-101:loxP-kanMX-loxP, matα), respectively. The diploid yeast cells were obtained using a mating protocol with both yeast strains.[86] These assays are based on the HIS3 reporter gene (growth assay without histidine).

Growth assay on +/− His plates

Interaction pairs were tested in duplicate as two independent diploid clones were picked for the growth assay. For each interaction, several dilutions (undiluted, 10^{-1}, 10^{-2}, 10^{-3}) of the diploid yeast cells (culture normalized at 5×10^{7} cells) and expressing both bait and prey constructs were spotted on several selective media. The DO-2 selective medium lacking tryptophan and leucine was used as a growth control and to verify the presence of both the bait and prey plasmids. The different dilutions were also spotted on a selective medium without tryptophan, leucine and histidine (DO-3) with and without methionine. Four different concentrations of 3-AT, an inhibitor of the HIS3 gene product, were added to the DO-3 plates to increase stringency. The following 3-AT concentrations were tested: 1, 5, 10 and 50 mM.

QUANTIFICATION AND STATISTICAL ANALYSIS

Quantification methods

All quantifications were done using ImageJ/Fiji[87] or Icy[88] software.

Densitometry analysis for Western blot was performed with ImageJ/Fiji. Pooled data from different replicate experiments were standardized as follows: ''normalized value (x) = (x – sample mean)/sample standard deviation''. To avoid negative numbers, the lowest value of all replicates was subtracted to the totality of values in the dataset. Note that in Figure 1H, the lowest value was set to 1 to better reflect the positive binding of all constructs.

For analysis of VGF signal distribution from confocal Z-stacks, cell bodies were manually selected in Icy and converted to 3D ROI. Large clustered perinuclear ($\geq2\mu m^3$) and small dispersed peripheral ($<2\mu m^3$) LAMP1+ populations were segmented by HK-means. VGF density signal was measured in these two compartments and normalized by the overall VGF density signal in cell bodies. Values of ''large'' and ''small'' values were added to give the total LAMP1+ structures.

For RUSH experiments with RUSH-VGF-mCherry, confocal Z-stacks were analyzed in ImageJ/FiJi and Icy. Each cell of interest (i.e., expressing both constructs without saturation and well spread), was manually picked and isolated as a single Z-stack using threshold in ImageJ/FiJi for further analysis. Then, per cell and over each Z-stack, signal of RUSH and GM130 were segmented by ''Spot detector'' and ''HK-Means'', respectively and RUSH integral intensity signal was measured in both regions of interest. A ratio (whole cell – GM130)/whole cell) RUSH signal was computed per cell and expressed as percentage. For RUSH experiments with mCherry-TNFα-SBP, after background correction, a Z-projection (SUM) was applied to each Z-stack. Masks of Golgi and whole cell were generated by thresholding the GM130 and mCherry staining, respectively and corresponding integral density signal was measured. Post-Golgi proportion of mCherry-TNFα-SBP signal was calculated from the following ratio: (whole cell – GM130)/whole cell.

Peripheral VGF signal in neurons was estimated using Icy software. In mCherry/RFP+ neurons, HK-means was applied to RFP signal to generate ''whole cell'' ROI while ''soma'' ROI was manually selected. Per cell, intensity of VGF was estimated in both ROI and plotted according to following ratio: (whole cell – soma)/whole cell.

Colocalization analysis was performed after cell selection on Z-stack with ''Colocalization Threshold'' plugin from ImageJ/Fiji.

Data representation and statistical analyses

Calculations were performed in Microsoft Excel. GraphPad Prism software (version 5.03) was used for graph generation and statistical analyses. Mean ± S.E.M of at least three independent experiments are shown. ANOVA with Tukey's post-tests were applied, as specified in the figure legends (*, $p < 0.05$; **, $p < 0.01$; and ***, $p < 0.001$; ns, not significant). Data were displayed as Superplots,[89] a color-coded manner to depict cell-level variability and experimental reproducibility. Figures were generated using open source Inkscape software. Graphical schemes were created with BioRender.com.